J|A|C|S
ARTICLES
Published on Web 04/05/2006

C_7 and C_9 Carbon-Rich Bridges in Diruthenium Systems: Synthesis, Spectroscopic, and Theoretical Investigations of Different Oxidation States

Stéphane Rigaut,*,† Céline Olivier,† Karine Costuas,† Sylvie Choua,‡ Omrane Fadhel,† Julien Massue,† Philippe Turek,‡ Jean-Yves Saillard,† Pierre H. Dixneuf,† and Daniel Touchard*,†

Contribution from the UMR 6226 CNRS − Université de Rennes 1, Sciences Chimiques de Rennes, Campus de Beaulieu, F-35042 Rennes Cedex, France, and the Institut Charles Sadron, UPR 22 CNRS − Université Louis Pasteur, 6 rue Boussingault, BP 40016, F-67083 Strasbourg Cedex, France

Received January 17, 2006; E-mail: stephane.rigaut@univ-rennes1.fr; daniel.touchard@univ-rennes1.fr

Abstract: Two methodologies of C−C bond formation to achieve organometallic complexes with 7 or 9 conjugated carbon atoms are described. A C_7 annelated *trans*-[Cl(dppe)$_2$Ru=C=C=C−CH=C(CH$_2$)−C≡C−Ru(dppe)$_2$Cl][X] (X = PF_6, OTf) complex is obtained from the diyne *trans*-[Cl(dppe)$_2$Ru−(C≡C)$_2$−R] (R = H, $SiMe_3$) in the presence of [$FeCp_2$][PF_6] or HOTf, and C_7 or C_9 complexes *trans*-[Cl(dppe)$_2$Ru−(C≡C)$_n$−C(CH$_3$)=C(R$_1$)−C(R$_2$)=C=C=Ru(dppe)$_2$Cl][X] (n = 1, 2; R$_1$ = Me, Ph, R$_2$ = H, Me; X = BF_4, OTf) are formed in the presence of a polyyne *trans*-[Cl(dppe)$_2$Ru−(C≡C)$_n$−R] (n = 2, 3; R = H, $SiMe_3$) with a ruthenium allenylidene *trans*-[Cl(dppe)$_2$Ru=C=C=C(CH$_2$R$_1$)R$_2$][X]. These reactions proceed under mild conditions and involve cumulenic intermediates [M$^+$]=(C=)$_n$CHR (n = 3, 5), including a hexapentaenylidene. A combination of chemical, electrochemical, spectroscopic (UV−vis, IR, NIR, EPR), and theoretical (DFT) techniques is used to show the influence of the nature and conformation of the bridge on the properties of the complexes and to give a picture of the electron delocalization in the reduced and oxidized states. These studies demonstrate that the C_7 bridging ligand spanning the metal centers by almost 12 Å is implicated in both redox processes and serves as a molecular wire to convey the unpaired electron with no tendency for spin localization on one of the halves of the molecules. The reactivity of the C_7 complexes toward protonation and deprotonation led to original bis(acetylides), vinylidene-allenylidene, or carbyne-vinylidene species such as *trans*-[Cl(dppe)$_2$Ru≡C−CH=C(CH$_3$)−CH=C(CH$_3$)−HC=C=Ru(dppe)$_2$Cl][BF_4]$_3$.

Introduction

Metal complexes which display ligand-mediated electronic effects, including electron-transfer phenomena, have attracted increasing interest.[1,2] The understanding and control of electron-transfer reactions constitute major challenges in science as it is a fundamental process to numerous complex chemical systems ranging from life processes[3] to electronic devices.[4,5] Electron-transfer processes between two redox centers have been examined with a range of linkers such as polyynes,[6−18] polyenes,[19] conjugated carboxylate,[20] polyaromatics,[1] or polypyridyl complexes.[1e,21] It appears from these studies that the nature of the ligand mediating the metal−metal interaction may be more relevant than the metal separation. Research in this area has mainly focused on the potential applications of these compounds in the preparation of molecular wires[1e,5−20] and dyes[22] and on unusual magnetic[23] or nonlinear optical[24] properties and quantum cell automata.[25] The building of bridges with unusual structures allowing communication between stable redox systems constitutes a potential source of applications.

A variety of organometallic molecules in which an even number of conjugated carbon atoms spans two metal fragments

† UMR 6226 CNRS − Université de Rennes 1.
‡ UPR 22 CNRS − Université Louis Pasteur.

(1) For reviews on electron transfer in mixed-valence systems, see: (a) Creutz, C. *Prog. Inorg. Chem.* **1983**, *30*, 1−73. (b) Brunschwig, B. S.; Creutz, C.; Sutin, N. *Chem Soc. Rev.* **2002**, *31*, 168−184. (c) Nelsen, S. F. In *Electron Transfer in Chemistry*; Balzani, V., Ed.; Wiley-VCH: Weinheim, Germany, 2001; Vol. 1, Chapter 10. (d) Launay, J.-P.; Coudret, C. In *Electron Transfer in Chemistry*; Balzani, V., Ed.; Wiley-VCH: Weinheim, Germany, 2001; Vol. 5, Chapter 1. (e) Launay, J.-P. *Chem. Soc. Rev.* **2001**, *30*, 386-397. (f) Demadis, K. D.; Hartshorn, C. M.; Meyer, T. J. *Chem. Rev.* **2001**, *101*, 2655−2685.
(2) Astruc, D. *Electron Transfer and Radical Processes in Transition Metal Chemistry*; VCH: New York, 1995.
(3) For example, see: (a) Lippard, S. J.; Berg, J. M. *Principles of Bioinorganic Chemistry*; University Science Books: Mill Valley, California, 1994. (b) Schuster, G. B. *Acc. Chem. Res.* **2000**, *33*, 253−260.
(4) (a) Wosnick, J. H.; Swager, T. M. *Curr. Opin. Chem. Biol.* **2000**, *4*, 715−720. (b) Tour, J. M.; Rawlett, A. M.; Kozaki, M.; Yao, Y.; Jagessar, R. C.; Dirk, S. M.; Price, D. W.; Reed, M. A.; Zhou, C.-W.; Chen, J.; Wang, W.; Campbell, I. *Chem.−Eur. J.* **2001**, *7*, 5118−5134. (c) Cahen, D.; Hodes, G. *Adv. Mater.* **2002**, *14*, 789−798. (d) *Molecular Electronics: Science and Technology*; Aviram, A., Ratner, M. A., Eds.; Annals of the New York Academy of Sciences, Vol. 852; New York Academy of Sciences: New York, 1998.
(5) (a) Lehn, J.-M. *Supramolecular Chemistry-Concepts and Perspectives*; VCH: Weinheim, 1995. (b) Ward, M. D. *Chem. Soc. Rev.* **1995**, *24*, 121−134. (c) McCleverty, J. A.; Ward, M. D. *Acc. Chem. Res.* **1998**, *31*, 842−851. (d) Tour, J. M. *Chem. Rev.* **1996**, *96*, 537−554. (e) Schwab, R. F. H.; Levin, M. D.; Michl, J. *Chem. Rev.* **1999**, *99*, 1863−1933. (f) *Atomic and Molecular Wires*; Joachim, C., Roth, S., Eds.; Kluwer: Dordrecht, The Netherlands, 1997.

in various structures such as sp carbon chains $M(C{\equiv}C)_nM$ with C_2 to C_{28} bridges were prepared and evaluated,[6−15] including complexes with an sp chain surrounded by sp^3 aliphatic carbon chains.[11] In contrast, considering the variety of available metallic fragments, only few complexes with an odd numbered carbon linear or cyclic bridge have been obtained, despite their highest interest for electron delocalization.[16,26−29] Long bridges with seven and more conjugated carbon atoms are particularly scarce,[7,29] due to a limited number of well-defined synthetic processes.

Using the fragment $[RuCl(dppe)_2]^+$ (dppe = 1,2-bis(diphenylphosphino)ethane) offering stable redox systems, our group has been involved in the building of new mono- and polymetallic complexes with unusual topologies, reversible redox behavior, that are potential molecular wires.[15] This system was first shown to be useful to afford metal cumulenylidenes *trans*-$[Cl(dppe)_2Ru{-}(=C)_n = CR_1R_2]^+$, acetylides *trans*-$[Cl(dppe)_2Ru{-}(C{\equiv}C)_n{-}R]$, and carbynes *trans*-$[Cl(dppe)_2Ru{\equiv}C{-}C{=}CR_1R_2]$, and it is now offering easy synthesis of bimetallic complexes containing bis-allenylidene, bis-acetylide, and bis-carbyne conjugated bridges.[30−32] Furthermore, a Ru(II) containing bis(allenylidene) bridge has been recently found to promote very efficient electronic communication between two carbon-rich chains.[33]

(6) (a) Bruce, M. I.; Low, P. J. *Adv. Organomet. Chem.* **2004**, *50*, 179−444. (b) Paul, F.; Lapinte, C. In *Unusual Structures and Physical Properties in Organometallic Chemistry*; Gielen, M., Willem, R., Wrackmeyer, B., Eds.; Wiley: New York, 2002; pp 220−291. (c) Szafert, S.; Gladysz, J. A *Chem. Rev.* **2003**, *103*, 4175−4206.

(7) (a) Antonova, A. B.; Bruce, M. I.; Ellis, B. G.; Gaudio, M.; Humphrey, P. A.; Jevric, M.; Melino, G.; Nicholson, B. K.; Perkins, G. J.; Skelton, B. W.; Stapleton, B.; White, A. H.; Zaitseva, N. N. *Chem. Commun.* **2004**, 960−961. (b) Bruce, M. I.; Ellis, B. G.; Low, P. J.; Skelton, B. W.; White, A. H. *Organometallics* **2003**, *22*, 3184−3198. (c). Bruce, M. I.; Low, P. J.; Costuas, K.; Halet, J.-F.; Best, S. P.; Heath, G. A. *J. Am. Chem. Soc.* **2000**, *122*, 1949−1962.

(8) (a) Paul, F.; Lapinte, C. *Coord. Chem. Rev.* **1998**, *178−180*, 431−509. (b) Le Narvor, N.; Toupet, L.; Lapinte, C. *J. Am. Chem. Soc.* **1995**, *117*, 7129−7138. (c) Roué, S.; Lapinte, C.; Bataille, T. *Organometallics* **2004**, *23*, 2558−2567. (d) Le Stang, S.; Paul, F.; Lapinte, C. *Organometallics* **2000**, *19*, 1035−1043. (e) Paul, F.; Meyer, W. E.; Toupet, L.; Jiao, H.; Gladysz, J. A.; Lapinte, C. *J. Am. Chem. Soc.* **2000**, *122*, 9405−9414. (f) de Montigny, F.; Argouarch, G.; Costuas, K.; Halet, J.-F.; Roisnel, T.; Toupet, L.; Lapinte, C. *Organometallics* **2005**, *24*, 4558−4572. (g) Bruce, M. I.; Costuas, K.; Davin, T.; Ellis, B. G.; Halet, J.-F.; Lapinte, C.; Low, P. J.; Smith, M. E.; Skelton, B. W.; Toupet, L.; White, A. H. *Organometallics* **2005**, *24*, 3864−3881.

(9) Sakurai, A.; Akita, M.; Moro-oka, Y. *Organometallics* **1999**, *18*, 3241−3244.

(10) (a) Dembinski, R.; Bartik, T.; Bartik, B.; Jaeger, M.; Gladysz, J. A. *J. Am. Chem. Soc.* **2000**, *122*, 810−822. (b) Brady, M.; Weng, W.; Zhou, Y.; Seyler, J. W.; Amoroso, A. J.; Arif, A. M.; Böhme, M.; Frenking, G.; Gladysz, J. A. *J. Am. Chem. Soc.* **1997**, *119*, 775−788. (c) Mohr, W.; Stahl, J.; Hampel, F.; Gladysz, J. A. *Chem.−Eur. J.* **2003**, *9*, 3324−3340. (d) Stahl, J.; Bohling, J. C.; Bauer, E. B.; Peters, T. B.; Mohr, W.; Martin-Alvarez, J. M.; Hampel, F.; Gladysz, J. A. *Angew. Chem., Int. Ed.* **2002**, *41*, 1872−1876. (e) Owen, G. R.; Stahl, J.; Hampel, F.; Gladysz, J. A. *Organometallics* **2004**, *23*, 5889. (f) Owen, G. R.; Hampel, F.; Gladysz, J. A. *Organometallics* **2004**, *23*, 5893−5895. (g) Zhuravlev, F.; Gladysz, J. A. *Chem.−Eur. J.* **2004**, *10*, 6510−6522. (h) Zheng, Q.; Gladysz, J. A. *J. Am. Chem. Soc.* **2005**, *127*, 10508−10509.

(11) Owen, G. R.; Stahl, J.; Hampel, F.; Gladysz, J. A. *Organometallics* **2004**, *23*, 5889.

(12) (a) Fernandez, F. J.; Blacque, O.; Alfonso, M.; Berke, H. *Chem. Commun.* **2000**, 1266−1267. (b) Kheradmandan, S.; Heinze, K.; Schmalle, H. W.; Berke, H. *Angew. Chem., Int. Ed. Engl.* **1996**, *35*, 2270−2273. (c) Kheradmandan, S.; Venkatesan, K.; Blacque, O.; Schmalle, H. W.; Berke, H. *Chem.−Eur. J.* **2004**, *10*, 4872−4885. (d) Fernandez, F. J.; Kheradmandan, S.; Venkatesan, K.; Blacque, O.; Alfonso, M.; Schmalle, H. W.; Berke, H. *Chem.−Eur. J.* **2003**, *9*, 6192−6206.

(13) (a) Xu, G.-L.; Zou, G.; Ni, Y.-H.; De Rosa, M. C.; Crutchley, R. J.; Ren, T. *J. Am. Chem. Soc.* **2003**, *125*, 10057−10065. (b) Ren, T. *Organometallics* **2005**, *24*, 4854−4870.

(14) Wong, K. T.; Lehn, J.-M.; Peng, S.-M.; Lee, G.-H. *Chem. Commun.* **2000**, 2259−2960.

(15) Rigaut, S.; Touchard, D.; Dixneuf, P. H. *Coord. Chem. Rev.* **2004**, 1586−16501.

(16) (a) Rigaut, S.; Le Pichon, L.; Daran, J.-C.; Touchard, D.; Dixneuf, P. H. *Chem. Commun.* **2001**, 1206−1207. (b) Rigaut, S.; Massue, J.; Touchard, D.; Fillaut, J.-L.; Golhen, S.; Dixneuf, P. H. *Angew. Chem., Int. Ed.* **2002**, *41*, 4513−4517.

(17) Gil-Rubio, J.; Werberndörfer, B.; Werner, H. *Angew. Chem., Int. Ed.* **2000**, *39*, 786−789.

(18) Hartbaum, C.; Mauz, E.; Roth, G.; Weissenbach, K.; Fischer, H. *Organometallics* **1999**, *18*, 2619.

(19) (a) Etzenhouser, B. A.; DiNiase Cavanaugh, M.; Spurgeon, H. N.; Sponsler, M. B. *J. Am. Chem. Soc.* **1994**, *116*, 2221−2222. (b) Etzenhouser, B. A.; Chen, Q.; Sponsler, M. B. *Organometallics* **1994**, *13*, 4176−4178. (c) Chung, M.-C.; Gu, X.; Etzenhouser, B. A.; Spuches, A. M.; Rye, P. T.; Seetharaman, S. K.; Rose, D. J.; Zubieta, J.; Sponsler, M. B. *Organometallics* **2003**, *22*, 3485−3494. (d) Liu, S. H.; Xia, H.; Wen, T. B.; Zhou, Z.; Jia, G. *Organometallics* **2003**, *22*, 737−743. (e) Liu, S. H.; Hu, Q. Y.; Xue, P.; Wen, T. B.; Williams, I. D.; Jia, G. *Organometallics* **2005**, *24*, 769−772.

(20) (a) Cotton, F. A.; Liu, C. Y.; Murillo, C. A.; Villagrán, D.; Wang, X. *J. Am. Chem. Soc.* **2004**, *126*, 14822−14831. (b) Cotton, F. A.; Donahue, J. P.; Murillo, C. A. *J. Am. Chem. Soc.* **2003**, *125*, 5436−5449. (c) Diketo, B.; Hoshino, Y.; Higushi, S.; Fielder, J.; Su, C.-Y.; Knölder, A.; Schwederski, B.; Sarkar, B.; Hartmann, H.; Kaim, W. *Angew. Chem., Int. Ed.* **2003**, *43*, 674. (d) Meacham, A. P.; Druce, K. L.; Bell, Z. R.; Ward, M. D.; Keister, J. B.; Lever, A. B. P. *Inorg. Chem.* **2003**, *42*, 7887−7896. (e) Kar, S.; Sarkar, B.; Ghumaan, S.; Janardanan, D.; van Slegeren, J.; Fielder, J.; Puranik, V. G.; Sunoj, R. B.; Kaim, W.; Lahiri, G. K. *Chem.−Eur. J.* **2005**, *11*, 4901−4911.

(21) (a) Baranof, E.; Collin, J.-P.; Flamini, L.; Sauvage, J.-P. *Coord. Chem. Rev.* **2004**, *33*, 147−155. (b) Welter, K.; Brunner, J.; Hofstraat, W.; De Cola, L. *Nature* **2003**, *21*, 54−57. (c) Ziesssel, R.; Hissler, M.; El-ghaoury, A.; Harriman, A. *Chem. Soc. Rev.* **1998**, *178−180*, 1251−1298. (d) Hofmeier, H.; Shubert, U. S. *Chem. Soc. Rev.* **2004**, *33*, 373−398. (e) Boyde, S.; Strouse, G. F.; Jones, W. E.; Meyer, T. J. *J. Am. Chem. Soc.* **1990**, *112*, 7395−7396. (f) Balzani, V.; Juris, A.; Venturi, M.; Campagna, S.; Serroni, S. *Chem. Rev.* **1996**, *96*, 759−833.

(22) (a) Wong, K. M.-C.; Lam, S. C.-F.; Ko, C.-C.; Zhu, N.; Yam, V. W.-W.; Roué, S.; Lapinte, C.; Fathallah, S.; Costuas, K.; Kahlal, S.; Halet, J.-F. *Inorg. Chem.* **2003**, *42*, 7086−7097. (b) Yam, V. W.-W.; Wong, K. M.-C.; Zhu, N. *Angew. Chem., Int. Ed.* **2003**, *43*, 1400−1403. (c) Lu, W.; Xiang, H.-F.; Zhu, N.; Che, C.-M. *Organometallics* **2002**, *21*, 2343−2346.

(23) Ung, V. A.; Cargill, W.; Thompson, A. M.; Bardwell, D. A.; Gatteschi, D.; Jeffery, J. C.; McCleverty, J. A.; Tolti, F.; Ward, M. D. *Inorg. Chem.* **1997**, *36*, 3447−3454.

(24) (a) Powell, C. E.; Humphrey, M. G. *Coord. Chem. Rev.* **2004**, *248*, 725−756. (b) Weyland, T.; Ledoux, I.; Brasselet, S.; Zyss, J.; Lapinte, C. *Organometallics* **2000**, *19*, 5235−5237. (c) Senechal, K.; Maury, O.; Le Bozec, H.; Ledoux, I.; Zyss, J. *J. Am. Chem. Soc.* **2002**, *124*, 4560−4561. (d) Long, N. J. *Angew. Chem., Int. Ed. Engl.* **1995**, *34*, 21−37. (e) Fillaut, J.-L.; Perruchon, J.; Blanchard, P.; Roncali, J.; Golhen, S.; Allain, M.; Migalsaka-Zalas, A.; Kityk, I. V.; Sahraoui, B. *Organometallics* **2005**, *24*, 687−695.

(25) (a) Qi, H.; Gupta, A.; Noll, B. C.; Snider, G. L.; Lu, Y.; Lent, C.; Fehlner, T. P. *J. Am. Chem. Soc.* **2005**, *127*, 15218−15227. (b) Qi, H.; Sharma, S.; Li, Z.; Snider, G. L.; Orlov, A. O.; Lent, C.; Fehlner, T. P. *J. Am. Chem. Soc.* **2003**, *127*, 15250−15259.

(26) (a) Bartik, T.; Johnson, M. T.; Arif, A. M.; Gladysz, J. A. *Organometallics* **1995**, *14*, 889−897. (b) Fischer, H.; Leroux, F.; Stumpf, R.; Roth, G. *Chem. Ber.* **1996**, *129*, 1475−1482. (c) Kolokova, N. Y.; Skripkin, V. V.; Alexandrov, G. G.; Struchkov, Y. T. J. *Organomet. Chem.* **1979**, *169*, 293−300. (d) Weng, W. J.; Berenguer, R.; Fornies, J.; Lalind, E.; Martinez, F.; Sanchez, L.; Serrano, B. *Organometallics* **1998**, *17*, 1640−1642. (e) Bullock, R. M. *J. Am. Chem. Soc.* **1987**, *109*, 8087−8089. (f) Roth, G.; Reindl, D.; Gockel, M.; Troll, C.; Fischer, H. *Organometallics* **1998**, *17*, 1393−1401. (g) Davison, A.; Solar, J. P. *J. Organomet. Chem.* **1978**, *155*, C8−C12. (h) Boland, B. E.; Fam, S. A.; Hughes, R. P. *J. Organomet. Chem.* **1979**, *172*, C25−C32. (i) Boland-Luissier, B. E.; Hughes, R. P. *Organometallics* **1982**, *1*, 635−639. (j) Leroux, F.; Stumph, R.; Fischer, H. *Eur. J. Inorg. Chem.* **1998**, 1225−1234.

(27) (a) Bartik, T.; Weng, W.; Ramsden, J. A.; Szafert, S.; Falloon, S. B.; Arif, A. M.; Gladysz, J. A. *J. Am. Chem. Soc.* **1998**, *120*, 11071−11081. (b) Dembinski, R.; Szafert, S.; Haquette, P.; Lis, T.; Gladysz, J. A. *Organometallics* **1999**, *18*, 5438−5440. (c) Fuss, B.; Dede, M.; Weibert, B.; Fischer, H. *Organometallics* **2002**, *21*, 4425−4431.

(28) (a) Jia, G.; Xia, H. P.; Wu, W. F.; Ng, W. S. *Organometallics* **1997**, *16*, 2940−2947. (b) Xia, H. P.; Ng, W. S.; Ye, J. S.; Li, X. Y.; Wong, W. T.; Lin, Z.; Yang, C.; Jia, G. *Organometallics* **1999**, *18*, 4552−4557. (c) Selegue, J. P. *J. Am. Chem. Soc.* **1983**, *105*, 5921−5923. (d) Jimenez Tenorio, M. A.; Jimenez Tenorio, M.; Puerta, M. C.; Velerga, P. *Organometallics* **1997**, *16*, 5528−5535.

(29) Hartbaum, C.; Fischer, H. *J. Organomet. Chem.* **1999**, *578*, 186−192.

(30) (a) Touchard, D.; Haquette, P.; Daridor, A.; Romero, A.; Dixneuf, P. H. *Organometallics* **1998**, *17*, 3844−3852. (b) Touchard, D.; Haquette, P.; Guesmi, S.; Le Pichon, L.; Daridor, A.; Toupet, L.; Dixneuf, P. H. *Organometallics* **1997**, *16*, 3640−3648. (c) Rigaut, S.; Monnier, F.; Mousset, F.; Touchard, D.; Dixneuf, P. H. *Organometallics* **2002**, *21*, 2654−2661.

(31) (a) Rigaut, S.; Perruchon, J.; Le Pichon, L.; Touchard, D.; Dixneuf, P. H. *J. Organomet. Chem.* **2003**, *670*, 37−44. (b) Rigaut, S.; Touchard, D.; Dixneuf, P. H. *Organometallics* **2003**, *22*, 3980−3984. (c) Rigaut, S.; Perruchon, J.; Guesmi, S.; Fave, C.; Touchard, D.; Dixneuf, P. H. *Eur. J. Inorg. Chem.* **2005**, 447−460.

(32) Mantovani, N.; Brugnati, M.; Gonsalvi, L.; Grigiotti, E.; Laschi, F.; Marvelli, L.; Peruzzini, M.; Reginato, G.; Rossi, R.; Zanello, P. *Organometallics* **2005**, *24*, 405−418.

This trans ditopic structure is of special interest to build oligomeric structures if the metal system allows trans communication between the carbon chains.[33−36]

The low availability of odd numbered chains led us to take profit of the $[RuCl(dppe)_2]^+$ system in the stabilization of carbon-rich metal complexes to develop new methodologies to build odd numbered carbon-rich bridged complexes and to investigate their electronic properties. Herein, we report on two novel methodologies of C−C bond formation to control the extension of an odd numbered carbon chain via the achievement of a class of bridged cationic carbon-rich homobimetallic complexes with seven conjugated carbons between remote metals with highly delocalized extended conjugated structures. The first one consists of an unprecedented radical or proton promoted coupling reaction occurring on the $C_\gamma{\equiv}C_\delta$ bond of a 1,3-diynylmetal derivative to lead to a complex $[Ru]^+{=}C{=}C{=}\overline{C{-}CH{=}C(CH_2)}{-}C{\equiv}C{-}[Ru]$ with a carbon-rich annelated C_8H_3 bridge. The second method describes the coupling between an allenylidene and a diynylmetal to provide $[Ru]{-}C{\equiv}C{-}C(CH_3){=}C(R_1){-}C(R_2){=}C{=}C{=}[Ru]^+$. This strategy allowed further access to the primary carbon-rich homonuclear bimetallic C_9 complex, which involves for the first time a hexapentaenylidene $[M^+]{=}C{=}C{=}C{=}C{=}C{=}CHR$ intermediate. We also report unprecedented detailed characterizations of odd numbered carbon bridged complexes in different oxidation states, and we provide a picture of the electron delocalization between two ruthenium termini using a combination of chemical, spectroscopic, and theoretical techniques, to improve the understanding of the ability of unsaturated odd numbered hydrocarbons to convey electrons in either an oxidation or a reduction process. In the last part of this work, we describe the reactivity of C_7 complexes that leads to original vinylidene-allenylidene or carbyne-vinylidene species. Unusual synthetic aspects of this work was presented in two communications.[16]

Results and Discussion

Synthesis of C_7 and C_9 Complexes. The discovery of this new type of bridges arises from our first attempts to couple two molecules of the mono-diynyl ruthenium *trans*-$[Cl(dppe)_2Ru{-}(C{\equiv}C)_2{-}H]$ (**2b**) in order to obtain a bimetallic RuC_8Ru complex in which eight carbon atoms span the metals as was achieved for the $RuC_{12}Ru$ complex with *trans*-$[Cl(dppe)_2Ru{-}(C{\equiv}C)_3{-}H]$.[31a] All oxidative coupling procedures to obtain RuC_8Ru were unsuccessful, and the formation of an unidentified product in the presence of copper(II) led us to consider the reactivity of the chemically oxidized species *trans*-$[Cl(dppe)_2Ru{-}(C{\equiv}C)_2{-}R]$ (**2a**: R = $SiMe_3$, **2b**: R = H). The most efficient reaction was observed with the addition of 0.5 equiv of ferrocenium hexafluorophosphate as oxidizing agent[37] to **2a**−**b** (Scheme 1). A formal [2 + 2] addition of the $C_\gamma{\equiv}C_\delta$ triple bonds takes place yielding dark purple crystals of [**3**][$\mathbf{PF_6}$]. The formation of [**3**][$\mathbf{PF_6}$] led us to imagine another possible route by protonation of **2a**−**b** to generate a $[Ru^+]{=}C{=}C{=}C{=}$CHR transient species. Indeed, a similar adduct [**3**][**OTf**] was obtained (70% yield) via addition of 0.5 equiv of strong acid (HOTf) to **2b**. The same reaction takes place on protonation of **2a**; thus spontaneous desilylation of **2a** occurs in the reaction medium, and previous deprotection is not necessary. NMR studies are consistent with a highly delocalized structure intermediate with those sketched in Scheme 1. Indeed, the ^{31}P analysis of [**3**][$\mathbf{PF_6}$] shows one singlet for the eight phosphorus nuclei, and the ^{13}C analysis shows only five different signals for the symmetric unsaturated bridge. Moreover, the Ru−C resonance at δ = 247.7 ppm (quint, ^2J(P,C) = 14 Hz) is downfield compared to that of an alkynyl (δ = 105.5 ppm for *trans*-$[Cl(dppe)_2Ru{-}C{\equiv}C{-}CPh_2H)]$)[30b] and upfield to that of an allenylidene complex (δ = 308.6 ppm for *trans*-$[Cl(dppe)_2Ru{=}C{=}C{=}CPh_2]$).[30a]

As a metallacumulene $[Ru^+]{=}C{=}C{=}C{=}$CHR intermediate is involved in the formations of both [**3**][**OTf**] and [**3**][$\mathbf{PF_6}$] (vide infra), we attempted to react the metal diyne systems **2a**−**b** with other preformed proton releasing cumulenic species such as ruthenium allenylidenes. Of interest here are the deprotonatable ruthenium allenylidene complexes of type *trans*-$[(dppe)_2(Cl)Ru{=}C{=}C{=}C(CH_2R_1)R_2]BF_4$ ([**4a**−**c**][$\mathbf{BF_4}$]) easily obtained using the Selegue's method,[38] on reaction of corresponding propargylic alcohol and of the 16-electron species $[(dppe)_2RuCl][BF_4]$ ([**1**][$\mathbf{BF_4}$]) (Scheme 2).

The neutral diynyl compound **2b** was added to 1 equiv of the cationic allenylidene complexes [**4a**−**c**][$\mathbf{BF_4}$], over a period of 3 days, at room temperature to lead to stable dark green crystals of [**5a**−**c**][$\mathbf{BF_4}$] isolated in good yields (79−85%). The addition should be slower than initially reported[16b] in order to minimize the formation of [**3**][$\mathbf{BF_4}$] as a side product (vide infra). These complexes **5a**−**c** were also obtained with similar yields when the reaction was performed with the protected diyne **2a**, without preliminary desilylation. The FTIR spectra for all compounds contain an intense absorption around 1900 cm^{-1}, characteristic of the cumulenic character of the chain. As observed for [**3**][$\mathbf{PF_6}$], the NMR spectra are consistent with a highly delocalized structure. The ^{31}P NMR analysis shows for [**5a**][$\mathbf{BF_4}$] one singlet at δ = 47.1 ppm for a symmetrical structure, and the ^{1}H NMR spectrum is composed of a single signal for two methyl groups at δ = 1.35 ppm. Conversely, NMR analysis evidences an unsymmetrical structure for the systems [**5b**][$\mathbf{BF_4}$] and [**5c**][$\mathbf{BF_4}$]. For example, in [**5c**][$\mathbf{BF_4}$], the ^{31}P NMR spectrum displays two singlets at δ = 43.8 and 49.6 ppm, and the ^{13}C NMR spectrum, seven different signals for the carbon chain assigned with the help of 2D HMBC and 2D HMQC experiments. The Ru−C carbon atom resonances

(33) Rigaut, S.; Costuas, K.; Touchard, D.; Saillard, J.-Y.; Golhen, S.; Dixneuf, P. H. *J. Am. Chem. Soc.* **2004**, *126*, 4072.
(34) (a) Lebreton, C.; Touchard, D.; Le Pichon, L.; Daridor, A.; Toupet, L.; Dixneuf, P. H. *Inorg. Chem. Acta* **1998**, *272*, 188−196. (b) Zhu, Y.; Clot, O.; Wolf, M. O.; Yap, G. P. A. *J. Am. Chem. Soc.* **1998**, *120*, 1812−1821.
(35) (a) Xu, G.-L.; De Rosa, M. C.; Crutchley, R. J.; Ren, T. *J. Am. Chem. Soc.* **2004**, *126*, 3728−3729. (b) Jones, S. C.; Coropceanu, V.; Barlow, S.; Kinnibrugh, T.; Timofeeva, T.; Marder, S. R. *J. Am. Chem. Soc.* **2004**, *126*, 11782−11783. (c) Schull, T. L.; Kushmerick, J. G.; Patterson, C. H.; George, C.; Moore, M. H.; Pollack, S. K.; Shashidhar, R. *J. Am. Chem. Soc.* **2003**, *125*, 3202−3203. (d) Stroh, C.; Mayor, M.; Von Hänisch, C.; Turek, P. *Chem. Commun.* **2004**, 2050−2051. (e) Mayor, M.; von Hänisch, C.; Weber, H. B.; Reichert, J.; Beckmann, D. *Angew. Chem., Int. Ed.* **2002**, *41*, 1183−1186. (f) Kuang, S.-M.; Fanwick, P. E.; Walton, R. A. *Inorg. Chem.* **2002**, *4*, 147−151.
(36) (a) Yip, J. H.; Wu, J.; Wong, K.-Y.; Ho, K. P.; Pun, C. S.-N.; Vittal, J. J. *Organometallics* **2002**, *21*, 5292−5300. (b) Sheng, T.; Varenkamp, H. *Eur. J. Inorg, Chem.* **2004**, 1198−1203. (c) Berry, J. F.; Cotton, F. A.; Murillo, C. A. *Organometallics* **2004**, *23*, 2503−2506. (d) Dewhurst, R. D.; Hill, A. F.; Willis, A. C. *Organometallics* **2004**, *23*, 1646−1648. (e) Zuo, J. L.; Herdtweck, E.; de Biane, F. F.; Santos, A. M.; Kühn, F. E. *New J. Chem.* **2002**, *26*, 883−888. (f) Weng, W.; Bartik, T.; Brady, M.; Bartik, B.; Ramsden, J. A.; Arif, A. M.; Glagysz, J. A. *J. Am. Chem. Soc.* **1995**, *117*, 11922−11931. (g) Zheng, Q.; Hampel, F.; Gladysz, J. A. *Organometallics* **2004**, *23*, 5896−5899.
(37) Connelly, N. G.; Geiger, W. E. *Chem. Rev.* **1996**, *96*, 877−910.
(38) Selegue, J. P. *Organometallics* **1982**, *1*, 217−218.

Scheme 1. Synthetic Pathways for C_7 and C_9 Bridged Complexes

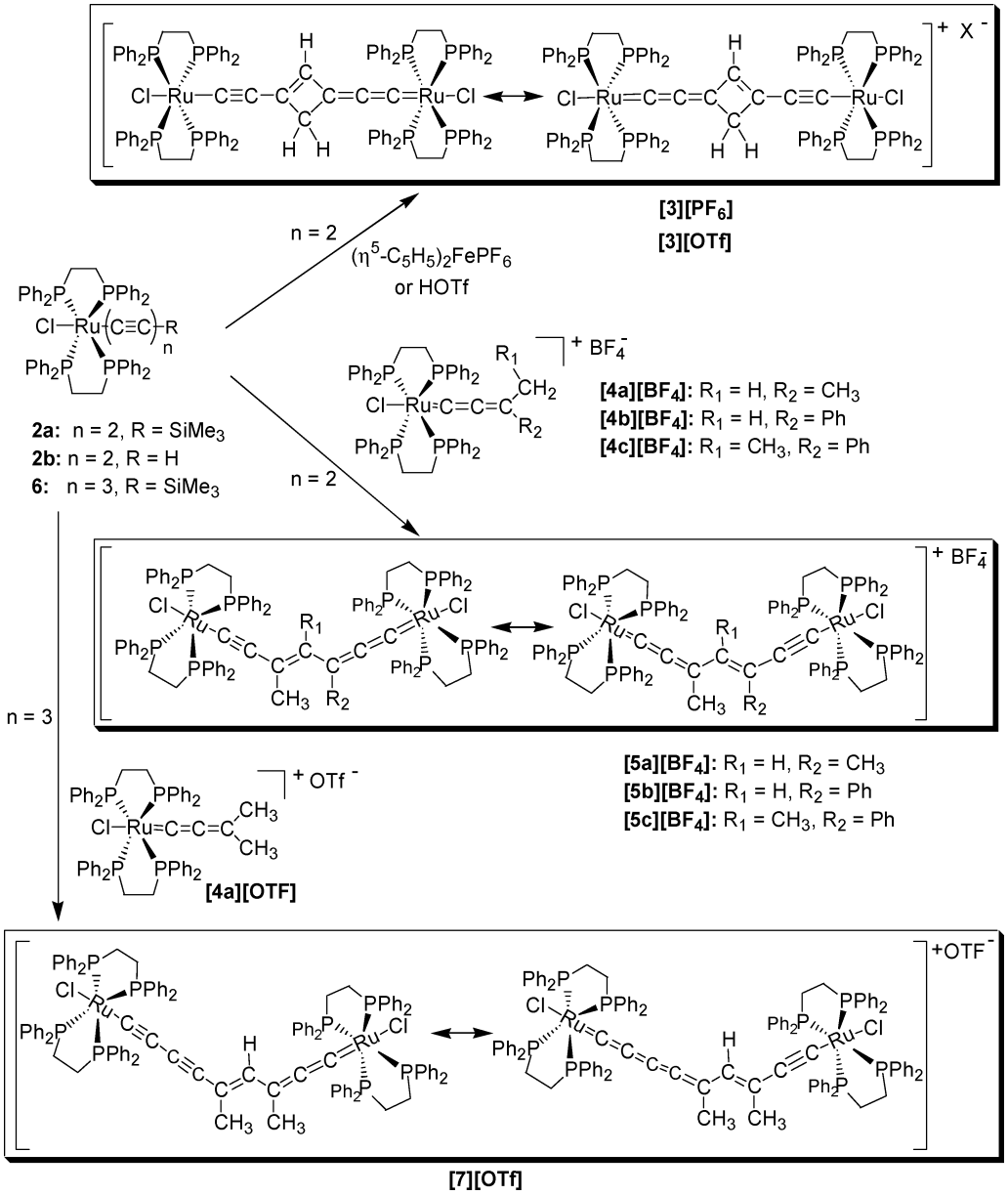

Scheme 2. Synthetic Pathway for Allenylidene Formations

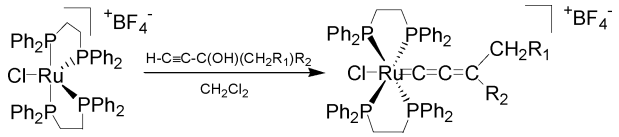

for these three compounds are also found intermediate between that of alkynyl and that of allenylidene complexes.

Three bridge configurations are possible for [**5a**−**c**][**BF**$_4$] owing to the three sp^2 carbons of the chain (Chart 1) and to the fact that form **IV** is very unlikely for steric reasons (see theoretical calculations). However, only one set of signals is observed for each compound. As free rotation is very improbable (see calculations), this indicates that only one form is detectable or that the NMR signals for the different forms are very close to each other. A further 2D NOESY experiment performed with [**5a**][**BF**$_4$] does not allow the observation of any correlation between the proton of the chain and the methyl group, which is rather in favor of the presence of the "w" shaped form **I**, as observed in the crystal structure (see below). For [**5c**][**BF**$_4$], if a very weak correlation signal between the central methyl group and the ortho hydrogen atoms of the chain phenyl is detected, a strong one between those aromatic protons and the other methyl group is observed. This result also evidences the "w" shaped form **I** as the preferred isomer with maybe a very small amount of form **III** not detected by other techniques. Finally for complex [**5b**][**BF**$_4$], no correlation is observed between the methyl group and the hydrogen atom of the chain, excluding the form **II**. As the protons of the chain phenyl group are not distinct from the dppe signals also correlated in space with the methyl group, we are not able to determine if we are in the presence of form **I** or **III**. It is of note that following our preliminary report, Bruce's group obtained recently related C_7

(39) Bruce, M. I.; Ellis, B. G.; Skelton, B. W.; White, A. H. *J. Organomet. Chem.* **2005**, *690*, 1772−1783.

Chart 1

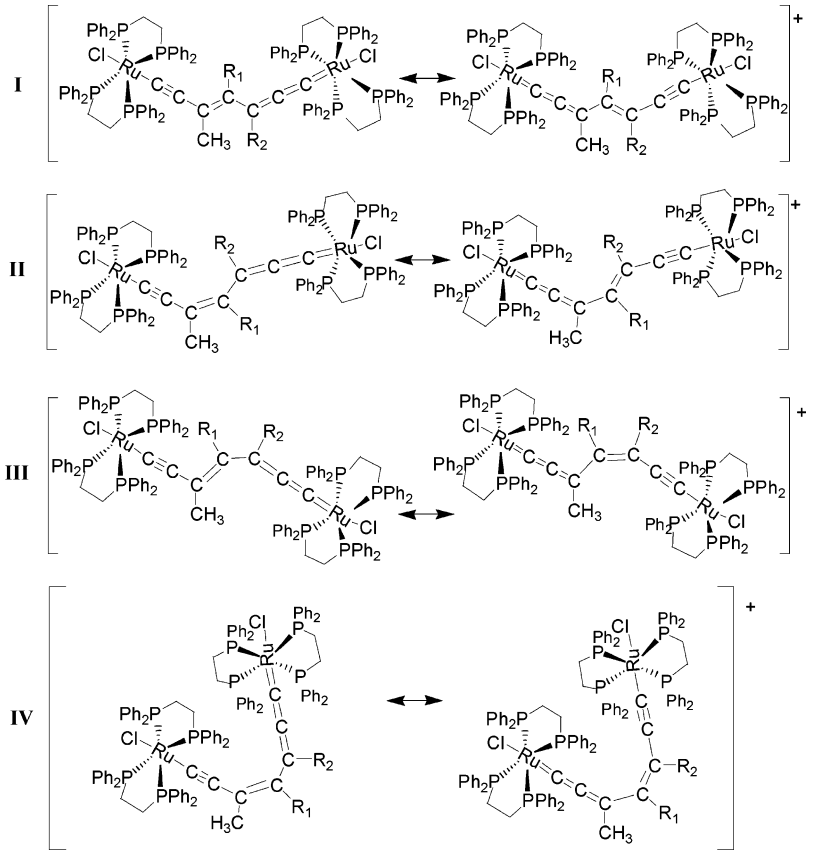

annelated and nonannelated compounds, in low yields or as traces, in the preparation of the acetylide [Cp*(dppe)Ru−C≡C−CO−CH_3].[39] In that case, the nonannelated complex [Cp*(dppe)Ru−C≡C−C(OCH_3)=C(H)−C(CH_3)=C=C=Ru(dppe)Cp*][PF_6], related to [**5a**][$\mathbf{BF_4}$], was present in two configurations and two sets of signals were observed in ^{13}C NMR spectra with a major contribution of "w" shaped configuration.

This novel pathway to make carbon−carbon bonds between the diynylmetal complexes **2a**−**b** and the allenylidene [**4a**−**c**][$\mathbf{BF_4}$] motivated the extension of the reaction to a longer polyyne. The procedure was applied to the triyne *trans*-[Cl(dppe)$_2$Ru−C≡C−C≡C−C≡C−$SiMe_3$](**6**) with the allenylidene [**4a**][**OTf**], in an attempt to also generate the first hexaheptaenylidene intermediate [M^+]=(C=)$_5$CHR on protonation of **6** by [**4a**][**OTf**] (see below). This quite slow reaction, 19 days at room temperature, with the triflate anion preferred for solubility reasons was successful and led to the bimetallic species [**7**][**OTf**] with nine conjugated carbon atoms between the two metal atoms in 49% yields (Scheme 1). The ^{1}H NMR spectrum is composed of a singlet at δ = 5.50 ppm for the proton on the chain and two signals for two methyl groups. The ^{31}P NMR analysis shows two singlets at δ = 48.4 and 43.9 ppm consistent with an unsymmetrical structure. Only one set of ^{1}H,^{31}P, and ^{13}C NMR signals is also observed here supporting the existence of only one privileged conformation to the chain. Nevertheless, we predict that the left mesomeric form represented in Scheme 1 is the most likely with an allenylidene and a diyne moiety. To our knowledge, this complex is the first one with nine conjugated carbon atoms spanning two identical metal moieties.

Crystal structures of [**3**][$\mathbf{PF_6}$] and [**5a**][$\mathbf{BF_4}$] could be resolved (Figure 1).[16] It is important to note that they both show analogous features that confirm an extended π-conjugation along the bridges as indicated by the NMR data. The Ru1−C1, C1−

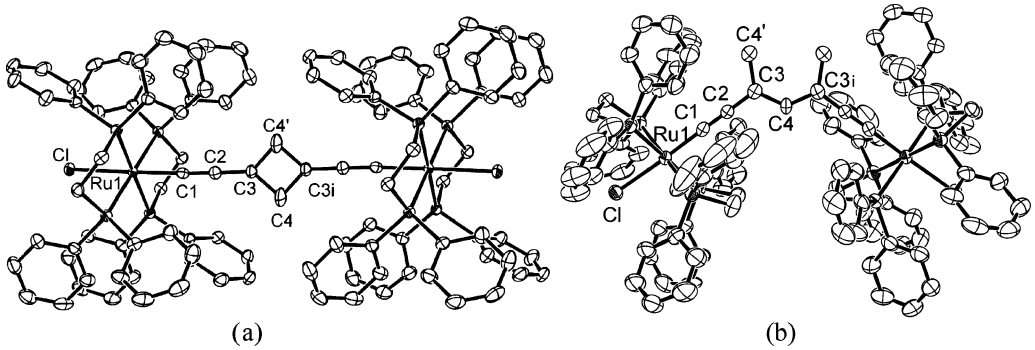

Figure 1. Molecular structure (ORTEP view) for (a) [**3**][$\mathbf{PF_6}$] and (b) [**5a**][$\mathbf{BF_4}$].

Table 1. Pertinent Optimized Bond Lengths (Å) for $[\mathbf{3}]^{n+}$, $[\mathbf{5a}-\mathbf{c}]^{n+}$ ($n = 0-2$) Compared Together with the X-ray Experimental Data in Italics;[16] See Figure 1 for Labelling[a]

	Ru1–C1	Ru1i–C1i	C1–C2	C1i–C2i	C2–C3	C2i–C3i	C3–C4	C3i–C4[b]	C3–C4′[c]	C3i–C4′/ C3i–C4′i[d]
3	2.030	2.035	1.249	1.247	1.384	1.384	1.412	1.412	1.547	1.547
$[\mathbf{3}]^{+}$	1.967	1.965	1.253	1.256	1.365	1.365	1.416	1.414	1.542	1.544
	1.933(3)		*1.225(4)*		*1.372(4)*		*1.457(5)*		*1.459(5)*	
$[\mathbf{3}]^{2+}$	1.946	1.948	1.263	1.262	1.362	1.362	1.411	1.411	1.549	1.550
5a-I	2.045	2.042	1.245	1.245	1.411	1.412	1.410	1.408	1.520	1.521
5a-II	2.040	2.042	1.245	1.243	1.406	1.412	1.412	1.404	1.515	1.519
$[\mathbf{5a\text{-}I}]^{+}$	1.988	1.986	1.253	1.253	1.391	1.391	1.410	1.410	1.515	1.515
	1.923(9)		*1.218(12)*		*1.390(13)*		*1.401(11)*		*1.528(12)*	
$[\mathbf{5a\text{-}II}]^{+}$	1.981	1.990	1.253	1.252	1.386	1.392	1.413	1.404	1.508	1.516
$[\mathbf{5a\text{-}I}]^{2+}$	1.959	1.958	1.261	1.261	1.386	1.386	1.417	1.418	1.511	1.511
$[\mathbf{5a\text{-}II}]^{2+}$	1.964	1.977	1.259	1.258	1.384	1.391	1.416	1.409	1.507	1.513
5b-I	2.034	2.039	1.244	1.245	1.411	1.412	1.405	1.412	1.516	1.495
5b-II	2.025	2.011	1.244	1.244	1.407	1.411	1.402	1.420	1.525	1.485
5b-III	1.999	2.010	1.245	1.242	1.407	1.412	1.407	1.410	1.517	1.489
$[\mathbf{5b\text{-}I}]^{+}$	1.983	1.989	1.253	1.253	1.390	1.392	1.412	1.408	1.512	1.499
$[\mathbf{5b\text{-}II}]^{+}$	1.957	1.902	1.261	1.262	1.388	1.379	1.403	1.424	1.522	1.488
$[\mathbf{5b\text{-}III}]^{+}$	1.920	1.928	1.261	1.261	1.381	1.385	1.419	1.406	1.508	1.503
$[\mathbf{5b\text{-}I}]^{2+}$	1.961	1.960	1.260	1.261	1.390	1.388	1.415	1.421	1.509	1.489
$[\mathbf{5b\text{-}II}]^{2+}$	1.957	1.902	1.261	1.262	1.388	1.379	1.403	1.424	1.522	1.488
$[\mathbf{5b\text{-}III}]^{2+}$	1.888	1.963	1.262	1.259	1.382	1.393	1.416	1.415	1.506	1.485
5c-I	1.945	2.006	1.245	1.246	1.410	1.414	1.420	1.429	1.517	1.496
5c-III	1.971	2.050	1.246	1.245	1.407	1.408	1.424	1.415	1.516	1.510
$[\mathbf{5c\text{-}I}]^{+}$	1.888	1.941	1.253	1.254	1.390	1.395	1.427	1.421	1.515	1.499
$[\mathbf{5c\text{-}III}]^{+}$	1.903	1.996	1.254	1.252	1.385	1.389	1.429	1.413	1.510	1.508
$[\mathbf{5c\text{-}I}]^{2+}$	1.843	1.899	1.268	1.266	1.382	1.387	1.437	1.439	1.512	1.493
$[\mathbf{5c\text{-}III}]^{2+}$	1.855	1.971	1.266	1.261	1.377	1.385	1.440	1.421	1.509	1.507

[a] Numbering of the X-ray structure of $[\mathbf{3}]^{+}$ and $[\mathbf{5a}]^{+}$ was extrapolated to the whole systems. [b] For $[\mathbf{3}]^{n}+$, C4 = CH. [c] For $[\mathbf{3}]^{n}+$, C4′ = CH_2; For $[\mathbf{5a}-\mathbf{c}]^{n}+$, C4′ = CH_3. [d] For $[\mathbf{3}]^{+}$, the distance C3i−C4′ is given; For $[\mathbf{5a}-\mathbf{c}]^{n+}$, the distance C3i−C4′i is given with C4′i = C(R2).

Scheme 3. Proposed Mechanisms for the Formation of the Annelated C_7 Complexes

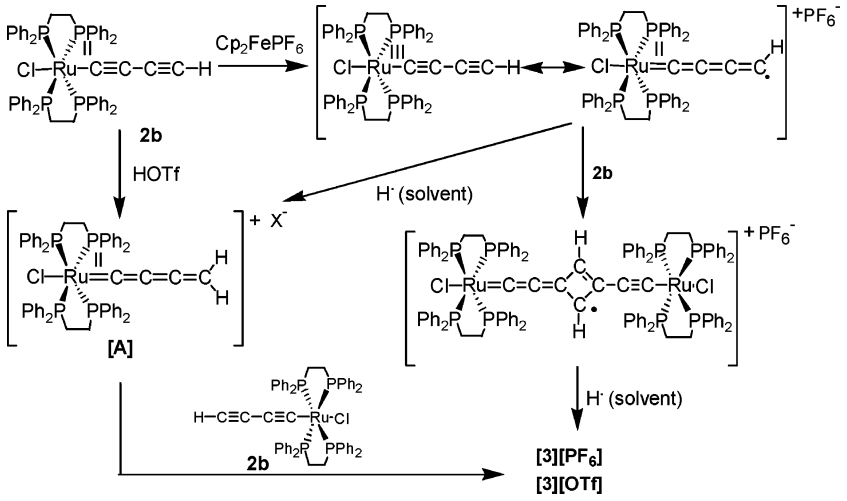

C2, C2−C3 distances (Table 1) are intermediate between respective typical values found in metal allenylidenes such as $[(\eta^5\text{-}C_5H_5)(PMe_3)_2Ru{=}C{=}C{=}CPh_2]PF_6$ [38] and metal alkynes such as $[Cl(dppe)_2Ru{-}C{\equiv}C{-}C_6H_4{-}p\text{-}NO_2]$.[40] With complex $[\mathbf{3}][\mathbf{PF_6}]$, the bridge arrangement is linear, and the four member ring is planar and symmetrical owing to a disorder.[41] For $[\mathbf{5a}]$-$[\mathbf{BF_4}]$, the structure is also symmetric, and the two ruthenium fragments are connected by a slightly twisted "W" shaped C_9H_7 bridge in order to minimize steric repulsions, supporting the presence of form **I** in solution. The different angles involving C3 and C4 are close to 120° showing the sp^2 nature of these carbon atoms, along with the C3−C4 bond length.

Reactions Mechanisms. The reaction mechanism to obtain $[\mathbf{3}][\mathbf{PF_6}]$ is not straightforward and was investigated. The protonation of **2b** should first lead to a cationic butatrienylidene intermediate [**A**] (Scheme 3), possibly via a vinylidene.[42] This is corroborated by our calculations on **2b** of which the HOMO is mainly and equally localized on C_β and C_δ. The latter is thus privileged to protonation for steric reasons. A further addition of the $C_\gamma{\equiv}C_\delta$ bond of another molecule **2b** on the resulting $C_\gamma{=}C_\delta$ bond of [**A**] is then proposed to lead to the annelated bimetallic complex [**3**][**OTf**]. Isolation of [**A**] has not been possible yet because of its high reactivity.[43,44] As a matter of

(40) Younus, M.; Long, N. J.; Raithby, P. R.; Lewis, J.; Page, N. A.; White, A. J. P.; Williams, D. J.; Colbert, M. C. B.; Hodge, A. J.; Khan, M. S.; Parker, D. G. *J. Organomet. Chem.* **1999**, *578*, 198−209.

(41) No H atoms could be located in the vicinity of C4 that accounts for the inversion centre; hence the four C−C bond lengths are identical within the ring.

(42) Koentjoro, O. F.; Rousseau, R.; Low, P. J. *Organometallics* **2001**, *20*, 4502−4509.

fact, the regioselectivity of the additions observed here is exceptional. The general process usually involves the most activated $C_\alpha{=}C_\beta$ bond of a vinylidene [M]=C=CHR or of an allenylidene [M=C=C=CR_1R_2] with the $C_\alpha{\equiv}C_\beta$ bond of a metal acetylide [M]−C≡C−R[26b−i] or of a polyyne.[26j] Indeed, this reaction was previously shown to afford rigid four membered cyclic bridges with a delocalized C_3 skeleton between metals and to inhibit the access to higher odd numbered carbon-rich bridges. Here, we assign the odd selectivity to the shielding of the $C_\alpha{-}C_\beta$ bonds by the bulky ruthenium moieties in the diyne complexes **2a**−**b** and [**A**], the $C_\gamma{-}C_\delta$ bonds being the most reactive. Indeed, the HOMO and LUMO of [**A**] show almost equal localization on $C_\alpha{=}C_\beta$ and $C_\gamma{=}C_\delta$.[58]

Concerning the oxidation route with the ferrocenium ion, we anticipate that, despite the unfavourable potential, the reaction is initiated by an electron transfer between ferrocenium and **2b** (E_{pa} = 0.13 V vs ferrocene, υ = 100 mV s^{-1}), followed by reaction of the resulting [**2b**]$^+$ with another molecule of **2b** (Scheme 3). This hypothesis is supported by the fact that the largest computed carbon spin density on **2b**$^+$ is on C_δ.[45] Additional incorporation of a hydrogen atom from the medium leads to [**3**][$\mathbf{PF_6}$]. An alternative route involves an earlier hydrogen incorporation to generate [**A**] from [**2b**]$^+$, and further reaction with another molecule of **2b** leads to [**3**][$\mathbf{PF_6}$] as in the protonation route.

A probable mechanism for the formation of [**5a**−**c**][$\mathbf{BF_4}$] also stands on the formation of the butatrienylidene intermediate [**A**]- and on the fact that ruthenium allenylidenes with a $-CH_2R_1$ group on C_γ are easily deprotonated into stable ruthenium acetylides *trans*-[$(dppe)_2$(Cl)Ru−C≡C−C(=CHR_1)R_2].[31b] This mechanism is depicted in Scheme 4 for **5b**. The first proposed step consists of the transfer of a proton from [**4b**][$\mathbf{BF_4}$] to the nucleophilic carbon C_δ of **2b** to form [**A**] and the acetylide **8b**. A further fast addition of the nucleophilic C_δ of **8b** on the electrophilic C_γ atom of [**A**] leads to the intermediate [**B**]. This is in agreement with a large localization of the LUMO of [**A**] on C_γ.[58] The formation of [**5b**][$\mathbf{BF_4}$] would then result from an allylic hydrogen transfer.[46] Two hydrogen atoms on one group on the $C\gamma$ of the allenylidene are required: one for the proton exchange between **2b** and [**4b**][$\mathbf{BF_4}$] and another one for the final transfer in [**B**].[47] When the reaction is carried out with the allenylidene *trans*-[$(dppe)_2$(Cl)Ru=C=C=(CH_2Ph)Ph]OTf ([**4d**]-[**OTf**]), the nucleophilic attack of the deprotonated species *trans*-[$(dppe)_2$(Cl)Ru−C≡C−C(=CHPh)Ph] (**8d**) and the subsequent formation of the analogue intermediate are not observed. Instead, the formation of [**3**][**OTf**] is observed as the result of the reaction of the cumulenic intermediate with another molecule of the diyne **2b**. The addition of nucleophile **8d** on [**A**] is certainly precluded for steric reasons, and recovering this acetylide (mixture of Z and E configurations) confirms the protonation reaction as the first step of the mechanism.[48]

The formation of the C_9 bridged complex [**7**][**OTf**] is expected to follow the same principle and is quite interesting to this point of view (Scheme 5). First of all, the protonation of the triyne **6** with the allenylidene [**4a**][**OTf**] should lead to an intermediate hexapentaenylidene species *trans*-[$(dppe)_2$(Cl)-Ru=C=C=C=C=C=CHSiMe_3)]$^+$ [**D**]. Further nucleophilic attack on the C_ϵ carbon atom of [**D**] by **8a**, the deprotonated form of [**4a**][**OTf**], provides [**7**][**OTf**] after a proton transfer. It is not clear whether desilylation occurs in the medium after or before the nucleophilic attack, but it is relevant that no attack is observed on the C_γ carbon otherwise some C_7 compound with a pendant triple bond would have been observed. From the orbital point of view, both attacks are equally probable, but the atomic charges favor C_ϵ addition.[58] To the best of our knowledge, this is the first evidence for the formation of a transient hexapentaenylidene species M=C=C=C=C=C=CR_1R_2. Indeed, while $L_nM{=}(C{=})_nCR_2$ species with n = 1 or n = 2 have already been widely investigated,[49] very few longer species n = 3[43] and 4[44] are known, and the intermediate formation of a higher heptahexaenylidene cumulene (n = 6) was postulated only once.[50]

Electronic Structure of [3]$^{2+/+/0}$ and [5a−b]$^{2+/+/0}$. To get a better understanding of the structure, reactivity, and properties of complexes [**3**]$^+$ and [**5a**−**c**]$^+$, we have undertaken DFT calculations with the help of the ADF code (see experimental part) on simplified models in which the phenyl groups of the dppe ligands have been replaced by hydrogen atoms. The monoreduced and mono-oxidized states of these models have also been computed. These time-consuming calculations were limited to the C_7 complexes, as oxidized and reduced forms of [**7**][**OTf**] are not stable (vide infra).

Four different isomers (**I**, **II**, **III**, **IV**) can be considered for the [**5a**−**c**]$^+$ compounds as shown in Chart 1. Preliminary calculations ruled out the possibility of the existence of isomer **IV**, due to high steric hindrance. [**5c-II**]$^+$ is highly unstable because of a strong repulsion between the two neighboring

(43) (a) Bruce, M. I. *Coord. Chem. Rev.* **2004**, *248*, 1603−1625. (b) Touchard, D.; Haquette, P.; Daridor, A.; Toupet, L.; Dixneuf, P. H. *J. Am. Chem. Soc.* **1994**, *116*, 11157−11159

(44) (a) This cumulene was successfully isolated only with Ir and with Mn complexes; see: Ilg, K.; Werner, H. *Angew. Chem., Int. Ed.* **2000**, *39*, 1632−1634. Venkatesen, K.; Fernandez, F. J.; Blacque, O.; Fox, T.; Alfonso, M.; Schmalle, H. W.; Berke, H. *Chem. Commun* **2002**, 2006−2007. (b) Touchard, D.; Dixneuf, P. H. *Coord Chem. Rev.* **1998**, *178*, 8−180, 409−429.

(45) The irreversible oxidation wave for **2b** confirms the high reactivity of the generated electrophilic organometallic radical [**2b**]$^+$ that should be the driving force of the reaction.

(46) This hypothesis is supported by ^{31}P NMR monitoring of the reaction that shows transient signals attributed to the intermediate [**B**] bearing an enynyl moiety (δ = 53.6 ppm) and an allenylidene moiety (δ = 43.2 ppm) and to the deprotonated complex **8b** (δ = 51.2 ppm).

(47) The proposed mechanism resembles those in the formation of an early bimetallic C_5 Ruthenium complex, but without cyclization owing to the bulky ligands. See: Selegue, J. P. *J. Am. Chem. Soc.* **1983**, *105*, 5921−5923.

(48) These observations are consistent with the fact that addition of the diyne on the allenylidene has to be as slow as possible in order to minimize the presence of **2b** in solution that could react with [**A**] to form [**3**]$^+$ as a byproduct.

(49) (a) Bruce, M. I. *Chem. Rev.* **1991**, *91*, 197−257. (b) Bruce, M. I. *Chem. Rev.* **1998**, *98*, 2797−2858. (c) Cardierno, V.; Gamasa, M. P.; Gimeno, J. *Eur. J. Inorg. Chem.* **2001**, 571−591. (d) Werner, H. *Chem. Commun.* **1997**, 903−910.

(50) Roth, G.; Fischer, H.; Meyer-Friedrichsen, T.; Heck, J.; Houbrechts, S.; Persoons, A. *Organometallics* **1998**, *17*, 1511−1516.

(51) Albright, T. A.; Burdett, J. K.; Whangbo, M.-H. In *Orbital Interactions in Chemistry*; John Wiley and Sons: New York, 1985.

(52) Lichtenberger, D. L.; Renshaw, S. K.; Bullock, R. M. *J. Am. Chem. Soc.* **1993**, *115*, 3276−3285.

(53) (a)Winter, R. F.; Hornung, F. M. *Organometallics* **1999**, *18*, 4005−4026. (b) Winter, R. F.; Klinkhammer, K. W.; Zalis, S. *Organometallics* **2001**, *20*, 1317−1333. (c) Hartmann, S.; Winter, R. F.; Sarkar, B.; Lissner, F. *J. Chem. Soc., Dalton Trans.* **2004**, 3273−3282. (d) McGrady, J. E.; Lovell, T.; Stranger, R.; Humphrey, M. G. *Organometallics* **1997**, *16*, 4004−4011.

(54) (a) Esteruelas, M. A.; Gomez, V. A.; Lopez, A.; Modrego, J.; Oñate, E. *Organometallics* **1997**, *16*, 5826−5835. (b) Cadierno, V.; Gamasa, M. P.; Gimeno, J.; González-Cueva, M.; Lastra, E.; Borge, J.; García-Granda, S.; Pérez-Carreño, E. *Organometallics* **1996**, *15*, 2137−2147.

(55) Barrière, F.; Camire, N.; Geiger, W. E.; Mueller-Westerhoff, U. T.; Sanders, R. *J. Am. Chem. Soc.* **2002**, *124*, 7262−7263.

(56) Creutz, C.; Chou, M. H. *Inorg. Chem.* **1987**, *26*, 2995−3000.

(57) Rigaut, S.; Maury, O.; Touchard, D.; Dixneuf, P. H. *Chem. Commun.* **2001**, 373−374.

(58) Auger, N.; Touchard, D.; Rigaut, S.; Halet, J.-F.; Saillard, J.-Y. *Organometallics* **2003**, *22*, 1638−1644.

Scheme 4. Proposed Mechanism for the Formation of the C_7 Complex [**5b**][BF_4]

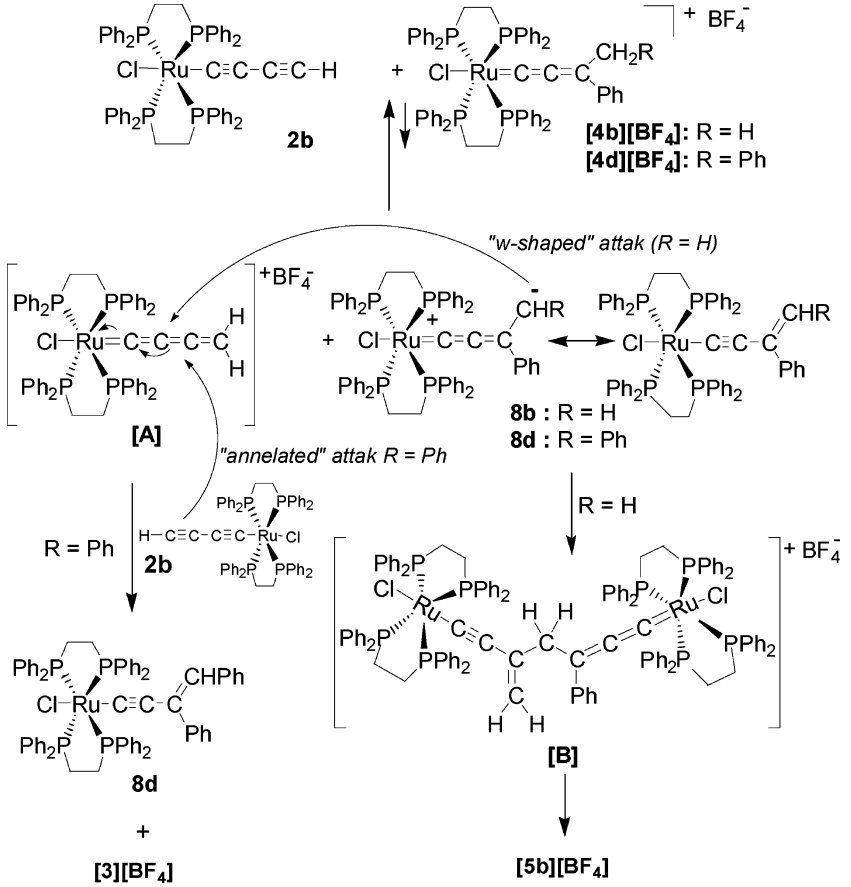

Scheme 5. Proposed Mechanism for the Formation of the C_9 Complex [**7**][**OTf**]

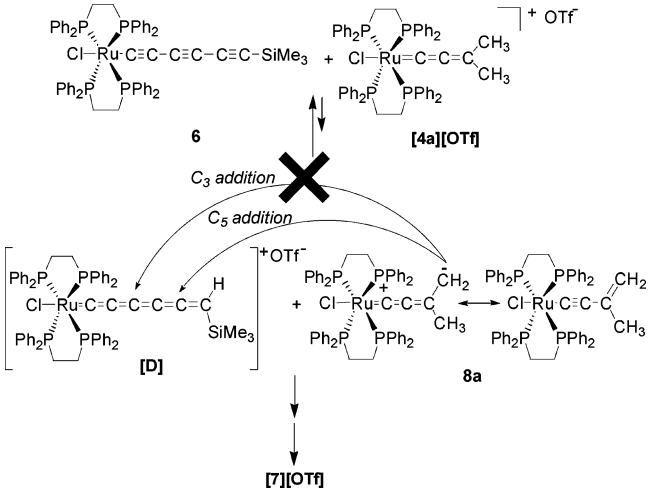

methyl groups and, thus, was not taken into account later on. This instability is not encountered in [**5b-II**]$^+$, the phenyl group being almost perpendicular to the conjugated chain, thus minimizing its repulsion with the methyl group. This preliminary conformational study allowed us to identify the systems to be considered, i.e., [**5a-I**]$^+$, [**5a-II**]$^+$, [**5b-I**]$^+$, [**5b-II**]$^+$, [**5b-III**]$^+$, [**5c-I**]$^+$, and [**5c-III**]$^+$ ([**5a-II**]$^+$ and [**5a-III**]$^+$ are identical (R^2 = CH_3)). The major optimized geometrical data computed for [**3**]$^{2+/+/0}$ and [**5a**−**c**]$^{2+/+/0}$ are reported in Table 1, together with the X-ray experimental values of [**3**][PF_6] and [**5a**][BF_4] given in italic.

Table 2. (A) Relative Energies for Each Species in Its Three Oxidation States, Given in eV; (B) Dipole Moments (given in Debye) Calculated for **3**, **5a**, **5b**, and **5c** in Their Different Geometries and Charges

	n		
	0	1	2
	(a) Relative Energies		
[**3**]$^{n+}$	−4.33	0.00	8.33
[**5a-I**]$^{n+}$	−4.03	0.11	8.46
[**5a-III**]$^{n+}$	−4.28	0.00	8.41
[**5b-I**]$^{n+}$	−4.36	0.00	8.39
[**5b-II**]$^{n+}$	4.27	0.16	8.55
[**5b-III**]$^{n+}$	−4.32	0.07	8.51
[**5c-I**]$^{n+}$	−4.14	0.20	8.71
[**5c-III**]$^{n+}$	−4.34	0.00	8.43
	(b) Dipole Moments		
[**3**]$^{n+}$	0.17	0.30	0.23
[**5a-I**]$^{n+}$	2.86	5.44	5.86
[**5a-III**]$^{n+}$	1.14	2.94	3.25
[**5b-I**]$^{n+}$	1.64	3.74	3.37
[**5b-II**]$^{n+}$	1.49	2.72	3.34
[**5b-III**]$^{n+}$	1.41	0.70	1.05
[**5c-I**]$^{n+}$	1.10	2.66	2.67
[**5c-III**]$^{n+}$	0.49	2.16	5.07

The relative energies and dipole moments computed for [**3**]$^{2+/+/0}$ and [**5a**−**c**]$^{2+/+/0}$ are reported in Table 2a and 2b. In [**5a**]$^{2+/+/0}$ and [**5c**]$^{2+/+/0}$ series, conformation **III** is calculated to be more stable in vacuum at 0 K. Conformation **I** is preferred over **III** in the [**5b**]$^{2+/+/0}$ series. Form **II** is much higher in energy. The energy difference between conformers is always lower than 0.30 eV. For example, [**5a**]$^+$ is 0.11 eV more stable in vacuum in its conformation III, but the dipole moment of

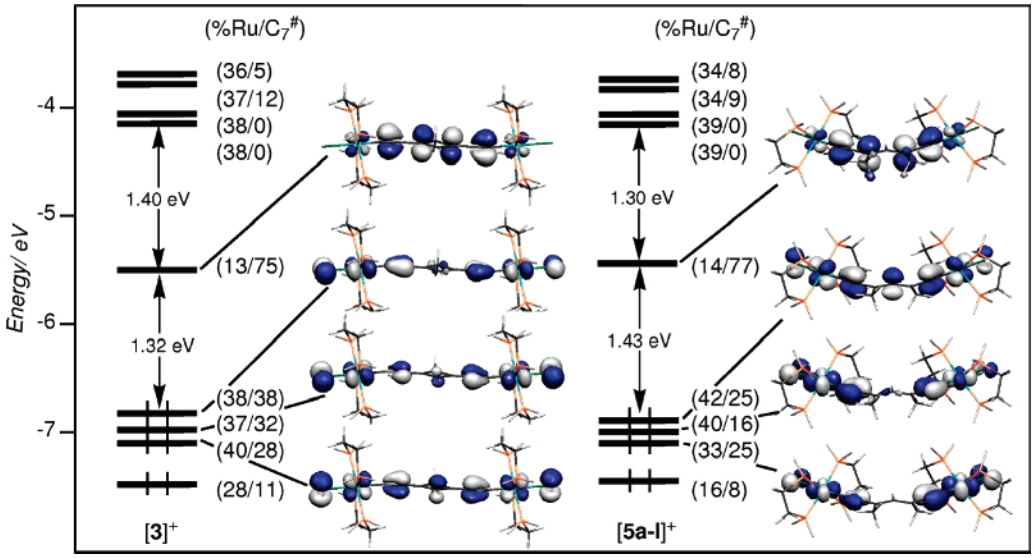

Figure 2. MO diagrams of $[\mathbf{3}]^+$ and $[\mathbf{5a}]^+$.

$[\mathbf{5a\text{-}I}]^+$ is much higher (5.44 vs 2.94 D, see Table 2), this suggesting a strong stabilization of this form in solution. Unfortunately, the wide range of calculated dipole moments prevents any conclusion concerning the conformation adopted in CH_2Cl_2 solution by those systems. The energy barrier needed to go from **III** to **I** was estimated to be 1.28 eV. An isomerization process is thus unexpected in solution, and this distribution must result from synthesis process. The X-ray and NMR measurements (vide supra) of $[\mathbf{5a}]^+$ reveal that the actual species is $[\mathbf{5a}-\mathbf{I}]^+$.This is also the case for $[\mathbf{5c}-\mathbf{I}]^+$ as evidenced by NMR data, with maybe some traces of isomer $[\mathbf{5c\text{-}III}]^+$. For $[\mathbf{5b}]^+$ the NMR measurements exclude form **II** but does not give any other information. However, in the light of what is observed with $[\mathbf{5a},\mathbf{c}]^+$, the differences in energy and in dipolar moment of **I** and **III**, we can reasonably consider that $[\mathbf{5b}-\mathbf{I}]^+$ is the form which is present in solution. Therefore, the "w" shaped isomer is assumed to be the actual conformation for the three complexes $[\mathbf{5a}-\mathbf{c}][\mathbf{BF_4}]$ in solution and in solid state, and only these conformations will be discussed later on. It has to be noted that **I** and **III** are electronically and structurally similar with $n = 1$ but also with $n = 0, 2$.

These calculations indicate no significant differences between the two molecular branches in the case of $[\mathbf{3}]^{2+/+/0}$ and $[\mathbf{5a}]^{2+/+/0}$ (as in the X-ray structures of and $[\mathbf{3}]^+$ and $[\mathbf{5a}]^+$) and small differences in the case of $[\mathbf{5b},\mathbf{c}]^{2+/+/0}$. This supports the view of equal weights for the two Lewis structures shown in Scheme 1 for $[\mathbf{3}]^+$ and $[\mathbf{5a}-\mathbf{c}]^+$ and full delocalization of the single electron in the case of $[\mathbf{3}]^{2+/0}$ and $[\mathbf{5a}-\mathbf{c}]^{2+/0}$. The optimized structures of $[\mathbf{3}]^+$ and $[\mathbf{5a}]^+$ are in good agreement with the experimental ones, with, as usually obtained with this type of calculations, slightly longer Ru−ligand distances. The optimized C1−C2 distances are also slightly longer. Moreover, the calculations on $[\mathbf{3}]^+$ allow us to distinguish between the $C(sp^2)-C(sp^2)$ and $C(sp^2)-C(sp^3)$ distances within the central C_4 ring, which are 1.414 Å and 1.544 Å, respectively. These values were not available from the X-ray data, due to structural disorder. As said above, the dissymmetry induced by the presence of R_2 substituents different from CH_3 on $[\mathbf{5b}]^+$ and $[\mathbf{5c}]^+$ has little effect on the π conjugated C_7 chain which remains almost symmetrical, the largest differences being, as expected, on the bonds involving the C3 atoms (~0.01 Å). The computed Mulliken atomic charges follow the same trend (see Supporting Information Table S1). Clearly, there is no significant tendency in $[\mathbf{5b}]^+$ and $[\mathbf{5c}]^+$ for a larger weight of one of the two Lewis structures of Scheme 1.

The MO diagrams of $[\mathbf{3}]^+$ and $[\mathbf{5a}]^+$ are sketched in Figure 2. The diagrams of $[\mathbf{5b}]^+$ and $[\mathbf{5c}]^+$ are very similar to those of $[\mathbf{5a}]^+$ and therefore are not shown here. A selection of frontier orbitals of $[\mathbf{3}]^+$ and $[\mathbf{5a}]^+$ is shown in Figure 2. It is clear that the electronic structures of $[\mathbf{3}]^+$ and $[\mathbf{5a}]^+$ are very similar. The presence of a strained C_4 ring of $[\mathbf{3}]^+$ is likely to destabilize the σ framework, but it merely perturbs the π-type system. There are two (one in-plane and one out-of-plane) $4d_\pi$ AOs per Ru atom. It results that in the dinuclear $[\mathbf{3}]^+$ and $[\mathbf{5a}]^+$ complexes, there are four MOs deriving from the four $4d_\pi$ AOs. These MOs are combinations of the so-called "t_{2g}" sets of the octahedrally surrounded Ru(II) atoms and therefore are occupied.[51] It turns out that these orbitals are the four highest occupied MOs of $[\mathbf{3}]^+$ and $[\mathbf{5a}]^+$ (Figure 2). They are the in-phase and out-of-phase combinations of the in-plane and out-of-plane $4d_\pi$ Ru AOs. As often observed in π-conjugated RuC_n complexes,[58] such $4d_\pi$ orbitals are mixed in an antibonding way with $\pi(C{=}C)$ levels. This is what happens in $[\mathbf{3}]^+$ and $[\mathbf{5a}]^+$, the four HOMOs of which exhibiting comparable antibonding Ru−C1 and bonding C1−C2 characters. These four MOs, which are also Ru−Cl antibonding,[52] differ mainly by their character on C4, since only the in-phase combinations of the RuC_3 moieties can mix with this atom by symmetry. Contrarily to their HOMOs which lie close in energy, the LUMOs of $[\mathbf{3}]^+$ and $[\mathbf{5a}]^+$ are isolated in the middle of a large energy gap (Figure 2). This suggests possible thermodynamical stability for some species which would have the same molecular structure and two more electrons than $[\mathbf{3}]^+$ and $[\mathbf{5a}]^+$. These LUMOs have little Ru participation (13% and 14%, respectively) and their largest coefficient on C3 and C3i (20 and 20% for $[\mathbf{3}]^+$, 21 and 21% for $[\mathbf{5a}]^+$). They exhibit bonding C1−C2 and antibonding C2−C3 character.

The mono-oxidation of $[\mathbf{3}]^+$ and $[\mathbf{5a}-\mathbf{c}]^+$ corresponds to the depopulation of the same HOMO (Figure 2). Consequently, the Ru−C1 and C1−C2 bonds are shortened and elongated, respectively (Table 1). As said previously, no tendency for spin localization on one of the halves of the molecule can be traced for the four complexes. A plot of the spin density of $[\mathbf{5a}]^{2+}$ is shown

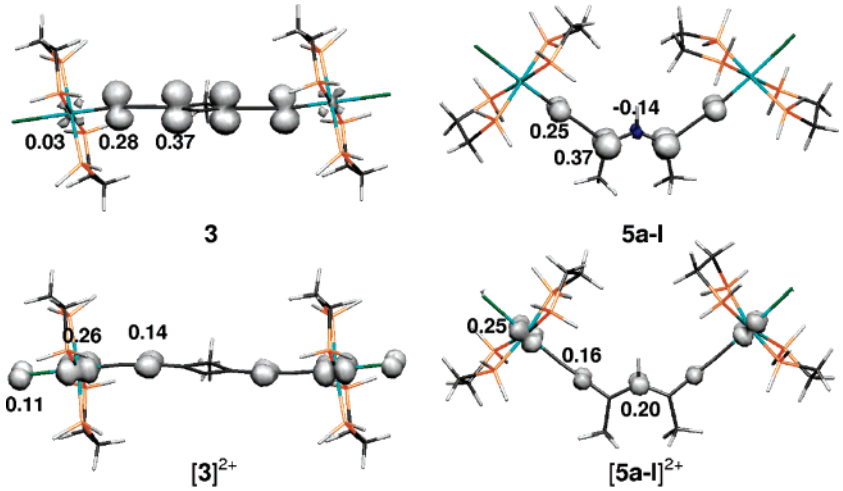

Figure 3. Contour plots of the calculated spin density of [**3**]$^{0,2+}$ and [**5a-I**]$^{0,2+}$; Contour values are ±0.0045 e/bohr^3.

Table 3. Atomic Spin Densities Calculated for **3**, [**3**]$^{2+}$, **5a**, [**5a**]$^{2+}$, **5b**, [**5b**]$^{2+}$, **5c**, [**5c**]$^{2+}$

	Ru1	Ru1i	C1	C1i	C2	C2i	C3	C3i	C4	C4′	C4′i	Cl1	Cl1i
3	0.03	0.03	0.28	0.28	−0.11	−0.11	0.37	0.37	−0.14	−0.04		0.00	0.00
[**3**]$^{2+}$	0.26	0.26	0.00	0.00	0.14	0.14	−0.02	−0.02	0.02	0.03		0.11	0.11
5a-I	0.03	0.03	0.25	0.25	−0.09	−0.09	0.37	0.37	−0.14	−0.02	−0.03	0.00	0.00
5a-II	0.02	0.03	0.22	0.27	−0.08	−0.10	0.36	0.40	−0.14	−0.03	−0.03	0.00	0.00
[**5a-I**]$^{2+}$	0.25	0.25	0.00	0.00	0.16	0.16	−0.07	−0.07	0.20	0.00	0.00	0.08	0.08
[**5a-II**]$^{2+}$	0.25	0.27	−0.02	−0.01	0.13	0.15	−0.06	−0.06	0.14	0.00	0.00	0.11	0.12
5b-I	0.03	0.03	0.24	0.25	−0.09	−0.09	0.35	0.36	−0.13	−0.03	−0.03	0.00	0.00
5b-II	0.03	0.02	0.25	0.22	−0.09	−0.08	0.35	0.33	−0.13	−0.03	−0.03	0.00	0.00
5b-III	0.02	0.03	0.20	0.25	−0.07	−0.09	0.32	0.37	−0.13	−0.02	−0.04	0.00	0.00
[**5b-I**]$^{2+}$	0.25	0.25	0.00	0.00	0.16	0.16	−0.06	−0.06	0.18	−0.06	−0.06	0.08	0.08
[**5b-II**]$^{2+}$	0.31	0.14	0.01	0.00	0.22	0.12	−0.04	−0.03	0.09	0.02	0.01	0.11	0.07
[**5b-III**]$^{2+}$	0.22	0.23	0.00	−0.01	0.19	0.15	−0.06	−0.06	0.18	0.00	0.01	0.08	0.10
5c-I	0.03	0.02	0.24	0.26	−0.08	−0.09	0.34	0.36	−0.13	−0.03	−0.03	0.00	0.00
5c-III	0.03	0.02	0.26	0.25	−0.09	−0.09	0.38	0.37	−0.13	−0.03	−0.02	0.00	0.00
[**5c-I**]$^{2+}$	0.18	0.20	0.02	0.02	0.19	0.19	−0.06	−0.06	0.21	0.01	0.01	0.04	0.04
[**5c-III**]$^{2+}$	0.19	0.24	0.00	0.00	0.17	0.16	−0.06	−0.06	0.18	0.00	0.00	0.07	0.10

in Figure 3. It fits nicely with the shape of the [**5a**]$^+$ HOMO (Figure 2). About half of the unpaired electron lies on the Ru centers. Table 3 shows that the atomic spin densities of all the computed bications are about the same. Similarly, the monoreduction of [**3**]$^+$ and [**5a**−**c**]$^+$ corresponds to the occupation of the same LUMO (Figure 2). It results in the Ru−C1 and C1−C2 bonds being elongated and shortened, respectively (Table 1). The plot of the spin density of **5a** nicely reproduces that of the LUMO of [**5a**]$^+$ (Figure 3). In particular, the Ru contribution is very small, most of the spin density being concentrated on the C3 and C1 atoms. Table 3 shows that all the computed reduced species exhibit similar spin distributions with no tendency for significant spin localization on one of the halves.

UV−Visible Spectra. In addition to classical intense short-wavelength absorption band for the n-π* type transitions originating from the dppe ligand at high energy below 300 nm (not shown), all complexes show a strong and broad band with a large extinction coefficient at lower energy (Table 4, Figure 4). The band presents a bathochromic shift from 633 nm with [**3**][**PF$_6$**] to 710 nm with [**5a**][**BF$_4$**]. Introduction of a phenyl group in [**5b**][**BF$_4$**] (λ_{max} = 746 nm) and [**5c**][**BF$_4$**] (λ_{max} = 764 nm) also contributes to the decrease in the absorption energy. Finally, the C_9 complex [**7**][**OTf**] shows a larger red shift than the C_7 analogue [**5a**][**BF$_4$**] attributed to the longer conjugation path but with a lower oscillator strength attributed to a weaker coupling between the metallic centers. Compounds [**5a**−**c**][**BF$_4$**] and [**7**][**OTf**] also exhibit weak absorptions at lower energy between 450 and 530 nm. In contrast, a higher energy band at 748 nm (shoulder) is observed for [**3**][**PF$_6$**].

Table 4. Cyclic Voltammetry and UV−vis Data for the Bimetallic Complexes

	electrochemistry[a]			UV–vis[f]
	E°_{red}[b]/V	E°_{ox1}[b]/V	E°_{ox2}/V	λ_{max}/nm (ϵ/mol^{-1} L cm^{-1})
[**3**]$^+$	−1.48	0.42	0.91[c]	633 (141 000) 748 (sh)
[**5a**]$^+$	−1.38	0.31	0.99[c]	455 (4000) 710 (127 600)
[**5b**]$^+$	−1.24	0.32	0.97[d]	494 (4700) 746 (98 000)
[**5c**]$^+$	−1.25	0.23	1.06[c]	502 (7600) 764 (109 000)
[**7**]$^+$	−1.16[d]	0.42[e]	0.96[c]	526 (14 600) 744(46 000)

[a] Sample, 1 mM; Bu_4NPF_6 (0.1 M) in CH_2Cl_2; υ = 100 mV s^{-1}; potentials are reported in volt vs ferrocene as an internal standard. [b] Reversible redox processes $\Delta E_p \approx 60$ mV, $I_{pc}/I_{pa} \approx 1$. [c] Peak potential of an irreversible process. [d] Partially reversible peak $\Delta E_p \approx 100$ mV, $I_{pc}/I_{pa} < 1$. [e] $\Delta E_p \approx 80$ mV. [f] In CH_2Cl_2, sh = shoulder.

For a monocumulenic compound such as the allenylidene *trans*-[Cl(dppe)$_2$Ru=C=C=CPh$_2$]PF$_6$, a transition with a λ_{max} value of 504 nm (ϵ = 18 000 mol^{-1} L cm^{-1}) is attributed to the allowed transition from the metal based HOMO-1 to the LUMO which is delocalized over the allenylidene ligand (the HOMO/LUMO symmetry is forbidden) and accounts for the strong Metal-to-Ligand Charge Transfer (MLCT).[53b] The intense bands observed here are very broad. The MO diagrams (Figure 2) suggest that they certainly include several transitions close in energy with an MLCT character. Clearly, if the λ_{max} values are highly influenced by the nature of the bridge, these

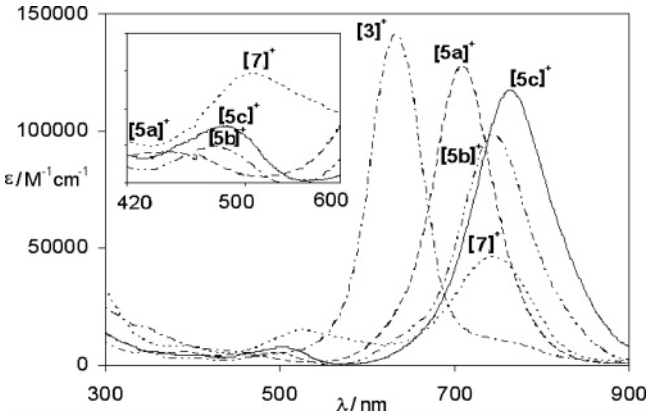

Figure 4. Electronic absorption spectra for [**3**][**PF$_6$**] (· − ·), [**5a**][**BF$_4$**] (− −), [**5b**][**BF$_4$**] (·· − ··), [**5c**][**BF$_4$**] (—), and [**7**][**OTf**] (· · ·) in CH_2Cl_2.

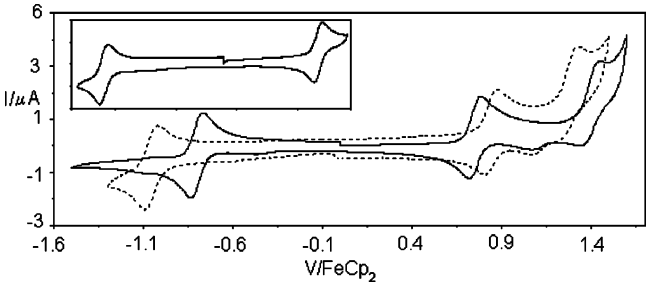

Figure 5. CV for [**3**]$^+$ (dashed) and [**5b**]$^+$ (plain); Bu_4NPF_6 (0.1 M) in CH_2Cl_2; v = 100 mV s^{-1}. Inset shows the full reversibility of the first oxidation process for [**3**]$^+$.

differences are difficult to rationalize on the basis of the MO diagrams and especially knowing the fact that the presence of a strained C_4 ring in [**3**][**PF$_6$**] does not significantly perturb the π-type system by comparison with [**5a**−**c**][**BF$_4$**] (vide supra). We attribute this phenomenon to the wide range of dipole moments (Table 2b) that preclude any simple analysis in polar solutions in which the complexes are soluble (CH_2Cl_2). Nevertheless, these bands are similar to that of conjugated bis-allenylidenes such as *trans*-[Cl(dppe)$_2$Ru═C═C═C(Ph)─C≡C─(Ph)C═C═C═RuCl(dppe)$_2$][CF_3SO_3]$_2$ (λ_{max} = 720 nm, ϵ = 60 000 mol^{-1} L cm^{-1}) or that of *trans*-[Cl(dppe)$_2$Ru─C≡C─*p*-(C_6H_4)─(Ph)C═C═C═RuCl(dppe)$_2$][CF_3SO_3] (λ_{max} = 764 nm, ϵ = 63 000 mol^{-1} L cm^{-1}).[31c] The latter with nine conjugated carbon atoms through a phenyl group presents a very similar spectrum to that of [**7**][**OTf**].

Electrochemical Data. These new bimetallic complexes are composed of several redox active units. To understand the nature of the redox behavior and the role of the linker, the cyclic voltammograms (CV) were recorded in CH_2Cl_2 solutions (0.1 M Bu_4NPF_6). The values of the potentials for all compounds are reported in Table 4. Typical CVs are displayed in Figure 5 for complexes [**3**]$^+$ and [**5b**]$^+$. All complexes exhibit a linear dependence of the peak current on the square root of the rate ($v^{1/2}$) from 60 to 600 mv s^{-1} as expected for a diffusion controlled process. They undergo a well-defined reversible one-electron oxidation wave followed by a partially reversible ([**5b**]$^+$) or irreversible ([**3**]$^+$, [**5a**]$^+$, [**5c**]$^+$, [**7**]$^+$) second oxidation consistent with an undergoing chemical reaction of the second oxidized species producing a new wave on the return scan around 1.08 V. A well-defined one-electron reversible reduction wave at a rather negative potential was also observed.

To a first approximation, the two oxidation steps are usually viewed as essentially involving the two Ru^{II}/Ru^{III} couples.[42,53−54] The unusually large separation of the processes ($\Delta E°$ = 650 mV, K_c = exp($\Delta E°F/RT$) = 1.50 × 10^{11} for [**5b**]$^+$) first establishes that all the mono-oxidized species are stable in solution with respect to disproportionation (mixed valence species)[8a,55] and supports the idea that they gain considerable stabilization due to delocalization. However, other phenomena such as columbic repulsion, structural distortion through the oxidations, and ion pairing besides delocalization also contribute to K_c, and one must therefore be careful in interpreting the meaning of K_c trends.[55] It is noteworthy that this value calculated for [**5b**]$^+$ is larger by several orders of magnitude than those found for the well-known Creutz−Taube ion {$Ru(NH_3)_5$}$_2$(μ-pyrazine) (K_c = 2.47 × 10^7, acetonitrile solution)[56] or for related species of comparable length such as [{Cp*(NO)(PPh_3)Re}$_2$-(μ-C_6)] (K_c = 3.0 × 10^6),[9a] [{Cp*(NO)(PPh_3)Re}$_2$(μ-C_8)] (K_c = 3.0 × 10^6), and [{Cp*(dppe)Fe}$_2$(μ-C_6)] (K_c = 5.9 × 10^4).[8a] The present value is of the order of magnitude of that of shorter C_4 species such as [{Cp*(NO)(PPh_3)Re}$_2$(μ-C_4)] (K_c = 1.1 × 10^9), [{Cp*(dppe)Fe}$_2$(μ-C_4)] (K_c = 1.6 × 10^{12}),[8b] [{Cp(PPh_3)$_2$-Ru}$_2$(μ-C_4)] (K_c = 1.5 × 10^{11}),[7c] [{Cp*(dppe)Fe}$_2$(μ-C_4H_4)] (K_c = 1.1 × 10^{12}),[19c] and [{I(dmpe)$_2$Mn}$_2$(μ-C_4)] (K_c = 5.4 × 10^{10}).[12b] Regarding the reduction wave at a rather negative potential, it is attributable at first glance to the reduction of the unsaturated carbon chain by analogy with other cumulenic complexes.[54,57−60] Although we can ascribe the origin of the redox processes (see below), calculated ionization potentials and electronic affinity fluctuations between the different C_7 complexes are not in agreement with the experimental trends. This is certainly the result of solvent and supporting electrolyte effects which are not taken into account in the calculations. Indeed, they are likely to be significant owing to the wide range of calculated dipole moments.

We can observe that these cationic bimetallic complexes are harder to oxidize than a neutral acetylide complex such as **2a** ($E°$ = 0.130 V vs $FeCp_2$) and easier to oxidize than a cationic allenylidene complex such as *trans*-[ClRu(dppe)$_2$═C═C═CPh_2]-PF_6 ($E°$ = 0.99 V vs $FeCp_2$). They are also harder to reduce than the latter ($E°$ = −1.03 V vs $FeCp_2$). These observations support a highly delocalized structure due to the nature of the bridge. It is noteworthy that the oxidation and reduction potentials of [**7**]$^+$ are respectively closer to that of acetylides and allenylidenes than that of [**5a**]$^+$. These easier reduction and harder first oxidation are the consequence of a longer conjugated bridge with a subsequent weaker interaction between the remote metals and indicate the more localized form with a positive charge on the allenylidene side as previously suggested. However, the charge in [**7**]$^+$ is more delocalized than that of the bimetallic *trans*-[Cl(dppe)$_2$Ru─C≡C─*p*-(C_6H_4)─(Ph)C═C═C═RuCl(dppe)$_2$][CF_3SO_3][31c] with nine carbon atoms to connecting two ruthenium atoms that display an oxidation and a reduction potential closer to those of the monometallic species owing to the aromatic character of the bridge.

Studies of the First Oxidized and Reduced Species. To collect more detailed information about those species, a series of spectroscopic experiments were carried out, covering the IR,

(59) (a) Re, N.; Sgamellotti, A.; Fioriani, C. *Organometallics* **2000**, *19*, 1115. (b) Marrone, A.; Re, N. *Organometallics* **2002**, *21*, 3562−3571.
(60) (a)Winter, R. F. *Eur. J. Inorg. Chem.* **1999**, 2121−2126. (b) Hartmann, S.; Winter, R. F.; Brunner, B. M.; Sarkar, B.; Knödler, A.; Hartenbach, I. *Eur. J. Inorg. Chem.* **2003**, 876−891.

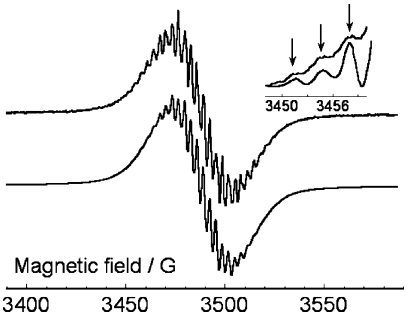

Figure 6. EPR spectrum of **5a** at 295 K in THF. Upper trace: experiment. Lower trace: computer simulation with $a^{31}_{P} = 6.3$ G (8 P), $a^{1}_{H} = 3.1$ G (1 H), $a^{99,101}_{Ru} = 3.9$ G (2 Ru), $g_{iso} = 2.0032$, 1.5 G line width. This hyperfine pattern is superimposed to a broad 1:1 Gaussian/Lorentzian component with a ca. 30 G line width to take account of all the unresolved structure. The inset shows that the satellite lines in the wings (low field part) are well reproduced upon comparing the simulated spectrum (lower trace, without the broad component) with the experimental one (upper spectrum) with this set of coupling constants.

NIR, visible, and UV regions of the spectrum on [**3**][**PF$_6$**] and [**5a**−**c**][**BF$_4$**] only, as [**7**][**OTf**] show very limited stabilities of the oxidized and reduced states. They were produced electrochemically (potential controlled electrolysis) by applying the potential corresponding to respective E_{pa} or E_{pc} values. EPR experiments were also performed on in situ chemically or electrochemically generated samples.

EPR Spectroscopy: Previous works have shown the efficiency of EPR spectroscopy to probe the electron distribution and the effective oxidation state of Ru complexes[61] including allenylidene derivatives.[31c−33,60] In the case of dinuclear derivatives, it is of particuliar interest to study the amount of electronic delocalization, assessing the electronic configuration between that of a mixed valence system Ru(II)−L−Ru(III) and that of a radical complex Ru(II)−L$^{\bullet}$−Ru(II).[31c,61a] The EPR spectra of binuclear Ru-radicals incorporating dppe show broad and usually unresolved features due to overlapping hyperfine contributions from ^{31}P, ^{99,101}Ru, and ^{1}H nuclei.[32,60b] Whatever the oxidation state in frozen solution, the principal values of the *g*-tensor may be used as a qualitative estimation of the extent of the electron over the metal and/or over the ligand upon checking the departure from the free electron *g*-value.[61a−c]

After reduction at room temperature of [**3**][**PF$_6$**] and [**5a**−**c**][**BF$_4$**] with cobaltocene ($E^{\circ} = -1.33$ V vs $FeCp_2$),[37,62] only the isotropic *g*-values in fluid solution could be estimated for the three resulting neutral species. These are very close to the free electron *g*-value: $g_{iso} = 2.0019$ (**5c**); $g_{iso} = 2.0032$ (**5a**); $g_{iso} = 2.0090$ (**3**), thus emphasizing the ligand centered reduction. Whereas the EPR spectrum of **3** shows no hyperfine structure, hyperfine features are detected for **5c** and **5a**, quite well resolved in the latter case (Figure 6). It is worth mentioning that similar observations (complex hyperfine pattern, $g_{iso} = 2.0048$) have been recently reported for mononuclear ruthenium allenylidene derivatives with phenyl groups in the carbon-rich fragment.[31c]

Inspection of the external lines in the wings of the EPR spectra could reveal in rare cases the hyperfine splitting (hfs) of Ru isotopes.[61a] This is suggested in the following, although the wings of the present spectrum are poorly resolved. If the electron is well delocalized over the two metal centers, the active set of nuclei being considered should be ^{31}P (8 P), ^{99,101}Ru (2 Ru), with the various combinations of isotopes, and ^{1}H (1 H). With these guidelines, the observed EPR spectrum of **5a** could be properly simulated (Figure 6). As mentioned, few ^{99,101}Ru hfs's have been reported in Ru based dinuclear complexes, and the present value 3.9 G is of the same order of magnitude as 4.35 G reported for a bis-Ru(3,6-bis(2-pyridyl)tetrazine) derivative.[61a] Most of the intensity of the spectrum (70%) is given by an underlying broad feature to represent all unresolved contributions (further H nuclei and anisotropic contributions). A value of $g_{iso} = 2.023$ has been recently reported[32] for a symmetrical bis-Ru(dppe) derivative comparable to **5a** but incorporating a bisanthracenylidene bridge instead of **(CH$_3$)**−**CH=C(CH$_3$)**. The present *g*-values for **3a** and **5a**,**c** derivatives are much closer to the free electron *g*-value, thus emphasizing a greater delocalization through the cumulene ligand. These results support the scheme of an electron mostly localized on the cumulene ligand with little contribution from the metal centers in a reduction process, according to previous observations of reduced bimetallic Fe−Ru centered allenylidene derivatives.[60b] The strong dependence of the electron delocalization on the nature of the central bridge between the Ru−allenylidene moieties is well emphasized.[31c,32]

Table 5. EPR Data (Principal Values of the *g*-Tensor) for [**3**]$^{2+}$, [**5a**]$^{2+}$, [**5c**]$^{2+}$

	g_1	g_2	g_3	$<g>^a$	g_1-g_3
[**3**]$^{2+}$	2.082	2.044	2.0007	2.043	0.081
[**5a**]$^{2+}$	2.078	2.020	1.918	2.0064	0.160
[**5c**]$^{2+}$	2.044	2.024	2.0005	2.023	0.044

[a] Calculated from $<g> = [(g_1^2 + g_2^2 + g_3^2)/3]^{1/2}$.

Studies of the first oxidized species [**3**]$^{2+}$, [**5a**]$^{2+}$, and [**5c**]$^{2+}$ were performed following the in situ electrolysis of the cationic derivative solutions at room temperature, by quenching and recording their EPR spectra at 77 K and 4 K. In fluid solution, the bications were EPR silent probably due to the spin−orbit contributions from the Ru nuclei being responsible for fast relaxation. Upon decreasing temperature from 77 K to 4 K, the intensity for all oxidized complexes increases. The three complexes exhibit slightly rhombic EPR spectra in frozen THF solution (see Supporting Information). Accordingly, these afford an estimation of the principal values of the *g*-tensor presented in Table 5. According to previous studies related to various Ru-allenylidene derivatives,[46a,b;61b,c] the quite low *g*-anisotropy estimated by (g_3-g_1) and the average $<g>$ factor being not strongly shifted from the free electron *g*-value do not favor a genuine metal centered oxidation. This conclusion is further supported by the fact that the EPR spectra are still observable at 77 K, hence showing an attenuated metallic character. As previously discussed,[61b] the *g*-anisotropy of dications with strong donor substituents decreases together with the contribution from the mixed-valent formulation Ru(II)−L−Ru(III).

UV−vis/IR/NIR Spectroscopies: One-electron electrochemical reductions were conducted only with [**5a**,**c**][**BF$_4$**], complex [**3**][**PF$_6$**] showing a limited stability on the electrolysis time scale.[63] Upon reduction, the discoloration of the mixtures and, thus, the vanishing of the intense visible bands with the development of a new broad band in the UV region character-

(61) (a) Kaim, W.; Ernst, S.; Kasack, V. *J. Am. Chem. Soc.* **1990**, *112*, 173−178. (b) Kasack, V.; Kaim, W.; Binder, H.; Jordanov, J.; Roth, E. *Inorg. Chem.* **1995**, *34*, 1924−1933. (c) Patra, S.; Sarkar, B.; Ghumaan, S; Fiedler, J.; Kaim, W.; Lahiri, G. K. *Dalton Trans.* **2004**, 754−758.

(62) The potentials of **3a** and **5a** are more negative compared to that of [$CoCp_2$]; however the values are close enough to observe a slight displacement of the equilibrium and to see the reduced species.

Table 6. UV−vis and NIR Data for $[\mathbf{3}]^{2+}$, $[\mathbf{5a}]^{2+}$, $[\mathbf{5c}]^{2+}$ in CH_2Cl_2

	UV–vis[a]	NIR[a]			
	λ_{max}/nm (ϵ/mol^{-1} L cm^{-1})	λ_{max}/nm/ν_{max}/cm^{-1} (ϵ/mol^{-1} L cm^{-1})	$\Delta\nu$ cm^{-1}	$\Delta\nu$ (calcd)[b] cm^{-1}	V_{ab}[c] eV
$[\mathbf{3}]^{2+}$	592 (39 700)	1432/6983 (3000)	1680	4016	0.43
$[\mathbf{5a}]^{2+}$	428 (6200), 614 (44 500)	1384/7225 (6300)	1270	4085	0.45
$[\mathbf{5c}]^{2+}$	484 (7300), 646 (31 000)	1367/7315 (5400)	1801	4110	0.45

[a] In CH_2Cl_2. [b] Calculated from $\Delta\nu_{1/2} = (2310\nu_{max})^{1/2}$ for symmetrical systems. [c] From $V_{ab} = \nu_{max}/2$.

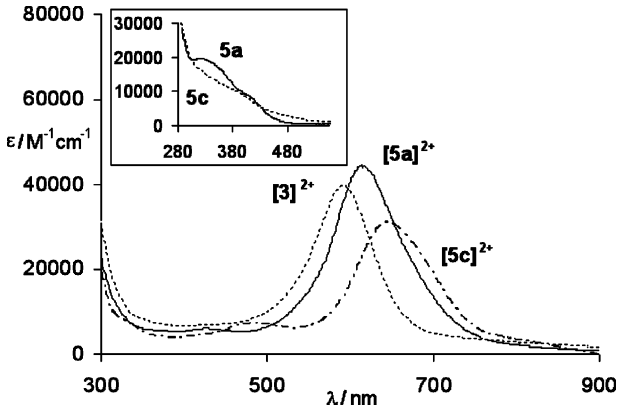

Figure 7. Electronic absorption spectra (CH_2Cl_2) of $[\mathbf{3}]^{2+}$ (· · ·), $[\mathbf{5a}]^{2+}$ (—), $[\mathbf{5c}]^{2+}$ (· − ·), inset shows the spectra for **5a** (—) and **5c** (· − ·).

istic of Ru(II) acetylides[53c,60b,64] were observed (inset, Figure 7). For **5a**, this new feature was detected at $\lambda_{max} = 311$ nm ($\epsilon = 19\,000$ mol^{-1} L cm^{-1}) with a shoulder on the low energy side at 390 nm. No bands were observed in the NIR region for both complexes after reduction. IR measurements in CH_2Cl_2 show the loss of the cumulenic band at 1906 cm^{-1} for **5a** and at 1895 cm^{-1} for **5c**, with the concomitant emergence of a weaker vibration stretch at 2049 cm^{-1} for the former symmetrical complex and of two vibrations at 2029 and 2045 cm^{-1} for **5c**. Added to EPR experiments, all these characteristics expected for ligand centered radical acetylides[31b,60] strongly support a reduction process mainly attributed to the reduction of the carbon chain with the single electron delocalized over the bridge. Furthermore, they are consistent with the above theoretical calculations, i.e., with the fact that the Ru−C1 (Ru−C′1) and C1−C2 (C′1−C′2) bonds are elongated and shortened, respectively, upon reduction and that most of the spin density is concentrated on the carbon chain (Table 3).

Electrochemical oxidations were performed on $[\mathbf{3}][\mathbf{PF_6}]$ and $[\mathbf{5a},\mathbf{c}][\mathbf{BF_4}]$.[63] IR studies show the vanishing of the cumulenic bands for all complexes, but the new vibration stretch intensities of the bridges are apparently too low to be observed, a fact already reported for other oxidized complexes.[12c,53a−b] For the three complexes, oxidation also leads to the disappearance of the intense band of the visible spectrum with the appearance of a significantly weaker band around 600 nm (Figure 7, Table 6). It is of note that, with $[\mathbf{5a}]^{2+}$ and $[\mathbf{5c}]^{2+}$, the weak bands are slightly blue shifted and a shoulder is no longer observed on the high energy side of the more intense band for $[\mathbf{3}]^{2+}$. Considering the ground-state electronic structure, these broad transitions might arise from several shifted MLCT or LMCT involving deeper occupied levels and the SOMO.

One-electron oxidations also give rise to an absorption band in the NIR region of the spectrum around 1400 nm (Figure 8, Table 6) which is characteristic of the formally mixed-valence nature of these compounds.[1,65] A relative sharp cutoff is

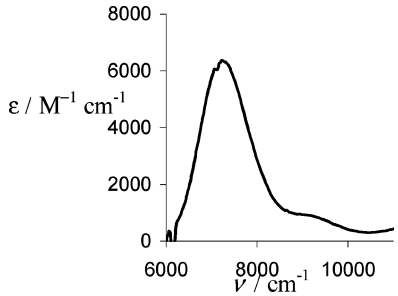

Figure 8. NIR absorption spectrum for $[\mathbf{5a}]^{2+}$ in CH_2Cl_2.

observed on the low energy side, while shoulders are detected on the high energy side. The presence of several NIR bands in the spectra of MV complexes is common and can be clearly related to the structure of the spacer or to the metal termini.[1f,8,9,19c] Assuming that the entire low NIR band represents the lowest energy band that should only be included in the calculation, and that the half width is not affected, analysis of the absorption for each complex yielded band data reported in Table 6.[66] The bandwidth of these transitions are far smaller than that predicted by the Hush model for the lowest energy IVCT electronic transition of symmetrical class II compounds ($\Delta\nu_{1/2} = (2310\nu_{max})^{1/2}$).[65] Together with the magnitude of the comproportionation constant and always keeping in mind that the bands are broadened by unresolved subbands, the characteristics of these bands are those of strongly coupled Robin and Day class III systems.[67] Similar measurements performed with $[\mathbf{5c}]^{2+}$ in THF[68] indicate a very weak shift from $\lambda_{max} = 1367$ nm (7315 cm^{-1}) to $\lambda_{max} = 1356$ nm (6711 cm^{-1}) with the polarity of the solvents also characteristic of a class III delocalized complex.

An exact assignment of the bands is ambiguous, but they are rather ascribed to $\pi-\pi$ bands of delocalized complexes than to intervalence transfer (IT) bands of localized (class II) ions. The lower energy band could be ascribed to the superexchange involving the bridging ligand's orbitals (from HOMO-1 to SOMO), whereas unresolved subbands to HOMO-n ($n > 1$) to SOMO transitions. The coupling parameters V_{ab} derived from the Hush theory for class III complexes (Table 6), and compared to those of class III analogues such as $[\{Cp^*(dppe)Ru\}_2(\mu\text{-}C_4)]$

(63) Reversibility was checked by back electrolysis that shows a recovering of the starting complexes superior to 90% on the basis of UV−vis and RMN experiments. Chemical reduction with 1 equiv of $[CoCp_2]$ in CH_2Cl_2 followed by reoxidation with 1 equiv of ferricinium salt 30 min later also led to the almost complete recovery of the starting complexes in the case of **5a**,**c** (>90%).

(64) Powell, C. E.; Cifuentes, M. P.; Morrall, J. P.; Stranger, R.; Humphrey, M. G.; Samoc, M.; Luther-Davies, B.; Heath, G. A. *J. Am. Chem. Soc.* **2003**, *125*, 602−610.
(65) Hush, N. S. *Prog. Inorg. Chem.* **1967**, *8*, 391−444.

(66) It is of note that in complex $[\mathbf{5c}]^{2+}$ the symmetry is slightly broken. Nevertheless, the characteristics are still very similar to those of the other complexes, suggesting also a completely delocalized compound to which we applied the same Hush treatment.

(67) Robin, M.; Day, P. *Adv. Inorg. Chem. Radiochem.* **1967**, *10*, 247−422.

(68) Similar measurements could not be conducted in more polar solvents such as methanol or acetonitrile for solubility or stability reasons.

(0.63 eV),[7b] [{Cp*(dppe)Fe}$_2$(μ-C$_4$)] (0.47 eV),[8a] [{Cp*(dppe)-Fe}$_2$(μ-C$_4$H$_4$)] (0.43 eV),[19c] and [{Cp*(dppe)Fe}$_2$(μ-C$_8$)] (0.32 eV),[8a] are other indications of the efficiency of these C$_7$ carbon-rich systems for electronic delocalization over a distance of almost 12 Å.[1d] This might be related to the presence of sp^2 carbon atoms in the chain, as MV species with double bonds display stronger coupling that analogous triple bonded species.[8a,19c,69] It is also worth noting that, except for [{Cp*-(dppe)Fe}$_2$(μ-C$_8$)], these previous studies with even numbered chains were limited to C$_4$ chains if no aromatic ring is present in the bridge[8e] because of the low stability of the paramagnetic species, as we observed with the C$_9$ species [**7**][**OTf**].

In conclusion to these oxidation processes, spectroscopic, EPR, and theoretical results point out the delocalized nature of the single electron in these oxidized C$_7$ species (Table 3) involving the two metallic centers with about half of the unpaired electron on the Ru atoms, and with an almost equal participation of the carbon bridge (C2, C2i, and C4). Therefore, the dissymmetry of the bridge does not induce the localization of the electron on one halve of the molecule toward class II complexes.

For several years now, it is well recognized that the structure of the mixed valence compound is highly dependent on the bridging ligand nature and on the metallic building blocks, the oxidation being less metal centered with ruthenium or rhenium complexes than with iron species.[8f] For example, Winter et al.[70] recently reported a bimetallic complex with a divinylphenylene bridge that dominates the anodic redox processes and that, as do the present results, also highlights that (1) the presence of the metal moieties endows the oxidized or reduced bridge with stabilities that are usually not encountered in their purely organic counterparts and (2) the bridge is a noninnocent redox ligand which cannot be decoupled from the metal in the redox processes.

Reactivity: Protonation and Deprotonation Reactions. The amphoteric behavior of allenylidene species bearing at least one methyl group on the C$_\gamma$ atom of cumulenic chain was previously reported.[31b] Deprotonation of the methyl group leads to an alkenyl acetylide while protonation on the C$_\beta$ atom provides an alkenyl carbyne group. As complexes [**3**][**PF$_6$**], [**5a**−**c**][**BF$_4$**], and [**7**][**OTf**] all display an allenylidene character and present protons on the C$_\delta$ positions, their protonation−deprotonation occurred to be an interesting field to investigate. The sequence was applied to the symmetrical compound [**5a**][**BF$_4$**] and to the unsymmetrical complex [**5c**][**BF$_4$**].[71]

First of all, deprotonation were performed using 1 equiv of DBU in CH$_2$Cl$_2$. The deeply colored cationic complexes [**5a**,**c**]-[**BF$_4$**] quickly led to pale yellow solutions consistent with the loss of the cumulenic character. In accord with Mulliken charges of [**5a**,**c**]$^+$ (Table S1), deprotonation occurs on the C$_\delta$ position to form the bis(acetylide) **9a**,**c**. However, the product is highly reactive, and attempts of purification to remove the salts led to the partial reprotonation. Nevertheless, the crude products were

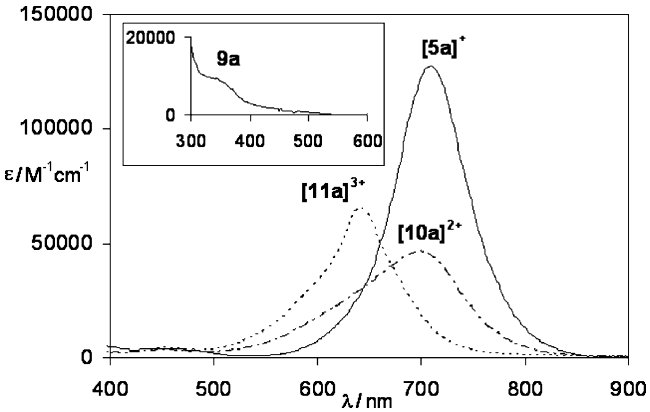

Figure 9. Electronic absorption spectra of [**5a**][**BF$_4$**] (—), [**10a**][**BF$_4$**]$_2$ (· — ·), [**11a**][**BF$_4$**]$_3$ (· · ·), and **9a** (inset) in CH$_2$Cl$_2$.

Table 7. UV−vis Data for Protonated and Deprotonated Species, in CH$_2$Cl$_2$

	UV–vis
	λ_{max}/nm (ϵ/mol^{-1} L cm^{-1})
9a	336 (9400)
9c	340 (9200)
[**10a**][**BF$_4$**]$_2$	454 (3100), 700 (45800)
[**10c**][**BF$_4$**]$_2$	494 (3500), 759 (32500)
[**11a**][**BF$_4$**]$_3$	454 (4000), 643 (65000)
[**11c**][**BF$_4$**]$_3$	494 (7500), 671 (34900)

satisfactorily identified. Considering **9a**, the ^{31}P analysis displays two resonances at δ = 51.0 and 49.8 ppm consistent with acetylide moieties. The most distinguishing features of the ^{1}H NMR data are the two coupled ethylenic hydrogen atoms on C$_\delta$, and the doublets are observed at δ = 4.70 and 4.65 ppm with ^2J(H,H) = 3.3 Hz. In addition, characteristic IR vibration stretches are observed, $\upsilon_{C\equiv C}$ = 2045 cm^{-1} and $\upsilon_{C=C}$ = 1645 cm^{-1}. Last, the intense absorption band disappears from the visible region with the development of a less intense low-energy shoulder superimposed on the absorptions of the aryl substituted phosphine ligands in the near UV region of the spectrum at ca. 340 nm, typical for Ru(II) acetylides (Figure 9, Table 7).[24a] Addition of 1 equiv of HBF$_4$·Et$_2$O in CH$_2$Cl$_2$ to **9a**,**c** led to the clean regeneration of [**5a**,**c**][**BF$_4$**].

By attempting to protonate the bimetallic compounds [**5a**,**c**]-[**BF$_4$**], we observed two stages of protonation on the two C$_\beta$ positions, in accord with Mulliken charges of [**5a**,**c**]$^+$ (Table S1) and the steric hindrance around C$_\alpha$. The first one occurs with 1 equiv of HBF$_4$·Et$_2$O owing to the acetylide character of the complexes and led to original blue-green vinylidene-allenylidene species [**10a**,**c**][**BF$_4$**]$_2$. For [**10c**][**BF$_4$**]$_2$, a broad vinylidene proton signal is observed at δ = 4.25 ppm, and the ^{31}P analysis displays two singlets at δ = 42.9 and 37.6 ppm for the allenylidene and vinylidene moieties, respectively. The Ru=*C* resonances at δ = 284.2 and 345.5 ppm (quint, $^2J_{PC}$ = 14 Hz) are also consistent with that attribution, the^{13}C analysis showing seven different signals for the unsaturated bridges. Two-dimensional ^{1}H−^{13}C NMR studies and analogies with other ruthenium complexes suggest that the allenylidene side is the one with the phenyl group. IR spectroscopy confirms the allenylidene character with a characteristic vibration stretch (1905 cm^{-1}).

The second protonation takes place on the other C$_\beta$ position to lead to deep blue carbyne-vinylidene complexes, with an

(69) For examples, see: (a) Ribou, A. C.; Launay, J.-P.; Sachtleben, M.; Li, H.; Spangler, C. W. *Inorg. Chem.* **1996**, *35*, 3735−3741. (b) Barlow, S.; Risko, C.; Chung, S.-J.; Tucker, N. M.; Coropceanu, V.; Jones, S. C.; Levi, Z.; Brédas, J.-L.; Marder, S. R. *J. Am. Chem. Soc.* **2005**, *127*, 16900−16911.

(70) Maurer, J.; Winter, R. F.; Sarkar, B.; Fiedler, J.; Zalis, S. *Chem. Commun.* **2004**, 1900−1901.

(71) The results of the reactions were not clear with the annelated [**3**][**PF$_6$**] and the C$_9$ [**7**][**OTf**] complexes leading to mixtures of unidentified products.

Scheme 6. Protonation and Deprotonation Sequences for [**5a,c**][BF_4].

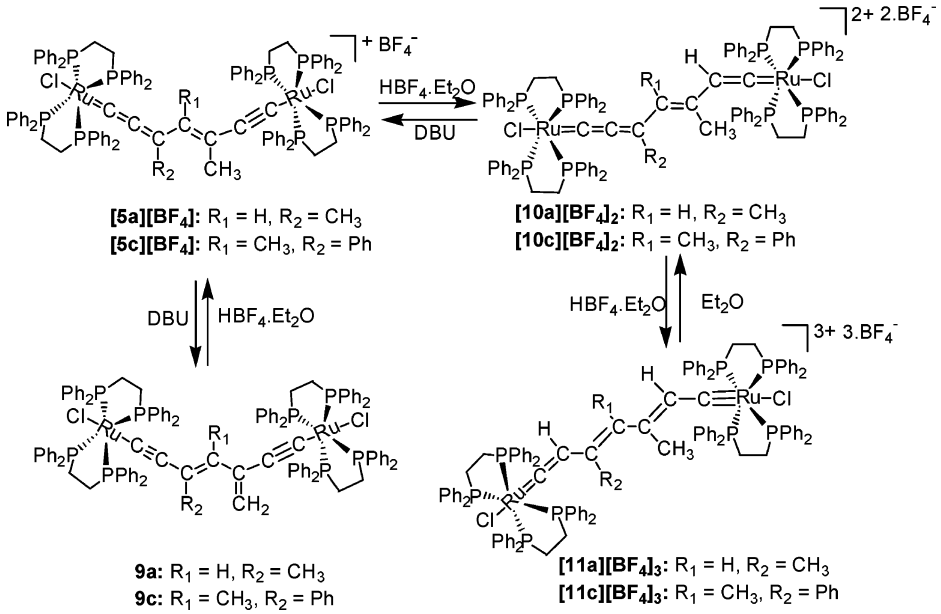

excess of $HBF_4 \cdot Et_2O$. The delocalized symmetrical structure of [**11a**][BF_4]$_3$ is supported by NMR evidence, and the actual formula is intermediate between the mesomeric form sketched in Scheme 6 and the other one giving the carbyne form to the other metal. Indeed, the ^{31}P NMR shows a singlet for the eight phosphorus atoms at high field (δ = 34.6 ppm), as expected for a carbyne contribution. The ^{1}H NMR spectrum displays a signal at δ = 5.95 ppm for the two β hydrogen atoms and one at −0.74 ppm for the methyl groups due to the shielding of the dppe ligands in close proximity.[31b] In the case of [**11c**][BF_4]$_3$, the carbyne function is rather localized on the methyl group side as evidenced by its high field ^{1}H methyl chemical shift (δ = −0.94 ppm), certainly for steric reasons.[31b] IR spectroscopy confirms the disappearance of the characteristic allenylidene vibration stretches, but no characteristic carbyne stretches were observed. The β proton is very acidic, and addition of a very weak base such as acetone or diethyl ether led to the regeneration of [**10a**,**c**][BF_4]$_2$. Therefore isolation the carbyne-vinylidene ruthenium was not possible. UV−vis studies show that the small high energy band of [**5a**,**c**][BF_4] is not markedly affected by the protonation processes and is maybe present in the deprotonated forms. In contrast, the low energy band is slightly shifted and less intense and displays a new shoulder on the high energy side after the first protonation (Figure 9, Table 7). The second one produces a more significant blue shift, as a consequence of the carbyne formation. These broad bands clearly include several transitions and are consistent with our previous observation on other carbyne species.[31b]

Conclusion. This work presents two easy methods to prepare cationic C_7 and C_9 carbon-rich bimetallic complexes with original topologies and a charge delocalized over the two metal centers, starting from simple polyyne and allenylidene precursors. The proposed mechanisms for these reactions arise from an unusual reactivity of the polyynyl ruthenium complexes that are protonated at the terminal carbon atom to generate a cumulenic intermediate, and especially the novel hexapentaenylidene species, reactive toward nucleophilic carbon-rich systems. The originality of these ruthenium complexes is that the terminal triple or double bond of polyynes and cumulene are the reactive sites, giving to these systems a high potential to build a variety of carbon-rich bridges for molecular wire systems. The nature and the stability of the bimetallic complexes allow their studies in different redox states for the first time with odd numbered species by means of EPR, IR, UV−vis, and NIR spectroscopies and computational studies (DFT). They established for the C_7 species that the more polar "w" shaped configuration is preferred for nonannelated compounds in the polar solvent in which the complexes are soluble. More importantly, they show (1) that in the reduced state the single electron is delocalized mainly over the carbon chain with very little metal contribution, whereas in the oxidized form the odd electron is fully delocalized over the chain and the metal centers (class III), over a distance of almost 12 Å, and (2) that all species exhibit similar spin distribution in each redox state with no tendency for spin localization on one of the halves. The reactivity toward protonation and deprotonation of some compounds was also examined and led to unique bis(acetylides), vinylidene-allenylidene, or carbyne-vinylidene species.

If the present work evidences that this kind of carbon chain serves as a molecular wire to delocalize the unpaired electron over the bridging ligand in an oxidation or a reduction process, it also confirms that a long chain with more than seven conjugated carbon atoms is not as suitable for a molecular wire given the high reactivity of the reduced and oxidized forms. As monometallic ruthenium complexes containing two carbon-rich chains have been found to promote very efficient electronic communication between the chains in either oxidation and reduction processes, the potential ability of this bimetallic system for trans chlorine atom substitution with an acetylide or a cumulenic chain makes them very attractive building blocks for one-dimensional nanoscaled organometallic conductive rod networks.

Experimental Section

General Comments. The reactions were carried out under an inert atmosphere using the Schlenk techniques. Solvents were freshly distilled under argon using standard procedures. TBAHP was recrystallized from methanol. Electrochemical studies were carried out under argon using an Eco Chemie Autolab PGSTAT 30 potentiostat (CH_2Cl_2, 0.1 M Bu_4-

NPF_6), the working electrode was a Pt disk, and ferrocene was the internal reference. EPR spectra were recorded with an ESP300E spectrometer (BRUKER) operating at X-band and equipped with a standard rectangular cavity (TE 102). An ESR900 cryostat (Oxford Instruments) was used for the low-temperature measurements. Computer simulations of the EPR spectra were performed with the help of Simfonia (BRUKER) and WINSIM (NIEH Public Software[72]) softwares. Prior to recording their EPR spectra, the singly oxidized complexes were generated in situ in a homemade cell. The electrolysis under argon atmosphere was performed at controlled potential with a three electrode configuration (platinum wire working electrode, platinum wire auxiliary electrode, and Ag wire as pseudo reference electrode). A dilute solution (ca. 10^{-3} M) of the precursor complexes was prepared with TBAHP (0.1 M) as the supporting electrolyte. The oxidation potentials were calibrated upon performing cyclic voltammetry before electrolysis. Neutral radicals were generated by chemical reaction at room temperature with cobaltocene. *cis*-$[(dppe)_2RuCl_2]$,[73] $[(dppe)_2RuCl][BF_4]$ (**[1][BF$_4$]**), $[(dppe)_2RuCl][OTf]$,[74] *trans*-$[Cl(dppe)_2Ru{-}C{\equiv}C{-}C{\equiv}C{-}SiMe_3]$(**2a**), *trans*-$[Cl(dppe)_2Ru{-}C{\equiv}C{-}C{\equiv}C{-}H]$(**2b**), *trans*-$[Cl(dppe)_2Ru{-}C{\equiv}C{-}C{\equiv}C{-}C{\equiv}C{-}SiMe_3]$(**6**),[31a] and $Ph(C_2H_5)C(OH){-}C{\equiv}CH$[75] were prepared as previously reported.

Computational Details: DFT calculations have been performed with the Amsterdam Density Functional package (ADF 2004.01).[76,77] Simplified molecules were used in order to reduce computational effort. The phenyl groups of the dppe ligands were replaced by hydrogen atoms. The geometries of **2b**, [**2b**]$^+$, [**3**]$^{n+}$, [**5a-I**]$^{n+}$, [**5b-I**]$^{n+}$, [**5c-I**]$^{n+}$, [**5b-II**]$^{n+}$, [**5a-III**]$^{n+}$, [**5b-III**]$^{n+}$, and [**5c-III**]$^{n+}$ (n = 0−2) were fully optimized without constraints (C_1 symmetry). This was done using the generalized gradient approximation potential BP86[78] and the analytical gradient method implemented by Verluis and Ziegler.[79] The atom electronic configurations were described by a triple-ζ Slater-type orbital (STO) basis set for H 1s, C 2s and 2p, and P 3s and 3p augmented with a 3d single-ζ polarization for C and P atoms and with a 2p single-ζ polarization for H atoms. A triple-ζ STO basis set was used for Ru 4d and 5s augmented with a single-ζ 5p polarization function for Ru. A frozen-core approximation was used to treat the core shells up to 1s for C, 2p for P, and 4p for Ru.[1] Spin-unrestricted calculations were performed for all the open-shell systems. Representations of the molecular structures and orbitals and spin densities were done using MOLEKEL4.3.[80]

***trans*-[Cl(dppe)$_2$Ru=C=C=C−CH=C(CH$_2$)−C≡C−Ru(dppe)$_2$Cl]-PF$_6$ ([3][PF$_6$]):** In a Schlenk tube, **2a** (527 mg, 0.5 mmol) and ferrocenium salt $[FeCp_2]PF_6$ (83 mg, 0.25 mmol) were dissolved in THF (50 mL). The solution was stirred during 8 h at room temperature. After filtration, the solution was evaporated, and then the residue was washed with diethyl ether. After crystallization in a dichloromethane/pentane mixture, 395 mg of dark purple crystals of [**3**][**PF$_6$**] were obtained (75%). $^{31}P\{^1H\}$ NMR ($CDCl_3$, 121.47 MHz, 297 K): δ = 44.81 (s., PPh_2), −143.95 (sept., $^1J(P,F)$ = 715 Hz). ^1H NMR ($CDCl_3$, 300.13 MHz, 297 K): δ = 7.47 to 7.02 (80H, Ph), 5.07 (s, 1H), 2.78 (m, 4H, PCH_2CH_2P), 2.65 (m, 4H, PCH_2CH_2P), 2.06 (s, 2H). $^{13}C\{^1H\}$ NMR ($CDCl_3$, 75.47 MHz, 297 K): δ = 284.4 (quint., Ru−C, $^2J(P,C)$ = 14 Hz), 166.40 (s, C2), 147.38 (s, C3), 139.88 (s, (CH)C4), 147.43−127.89 (Ph), 49.02 (s, $(CH_2)C4'$), 30.32 (m, PCH_2CH_2P, $|^1J(P,C) + {}^3J(P,C)|$ = 23 Hz). IR (KBr): υ = 1909 (s., =C=C=C), 838 (s., PF) cm^{-1}. HR-MS FAB$^+$ (*m*/*z*): 1965.3107 ([M]$^+$, calcd: 1965.3112).

***trans*-[Cl(dppe)$_2$Ru=C=C=C−CH=C(CH$_2$)−C≡C−Ru(dppe)$_2$Cl]-OTf ([3][OTf]):** In a Schlenk tube containing **2a** (300 mg, 0.3 mmol) in CH_2Cl_2 (10 mL), a solution of triflic acid (15 μL, 0.16 mmol) in CH_2Cl_2 (10 mL) was added. The solution was stirred during 16 h at room temperature. The solution was evaporated, and the residue was washed with diethyl ether (3 × 25 mL). After crystallization in a dichloromethane/pentane mixture, 225 mg of dark purple crystals of [**3**][**OTf**] were obtained (71%). $^{31}P\{^1H\}$ NMR ($CDCl_3$, 121.47 MHz, 297 K): δ = 44.58 (s., PPh_2). ^1H NMR ($CDCl_3$, 300.13 MHz, 297 K): δ = 7.50 to 7.05 (80H, Ph), 5.10(s, 1H), 2.82 (m, 8H, PCH_2CH_2P), 2.13 (s, 2H). $^{13}C\{^1H\}$ NMR ($CDCl_3$, 75.47 MHz, 297 K): δ = 284.55 (quint., Ru−C, $^2J(P,C)$ = 14 Hz), 166.52 (s, C2), 147.44 (s, C3), 139.95 (s, (CH)C4), 147.39−127.87 (Ph), 49.07 (s, $(CH_2)C4'$), 30.38 (m, PCH_2-CH_2P, $|^1J(P,C) + {}^3J(P,C)|$ = 23 Hz). IR (KBr): υ = 1908 (s., = C= C=C) cm^{-1}; HR-MS FAB$^+$ (*m*/*z*): 1965.3126 ([M]$^+$, calcd: 1965.3112).

Alternative Route to [3][OTf] with [4d][OTf]: In a Schlenk tube, **2a** (300 mg, 0.3 mmol) and [**4d**][**OTf**] (192 mg, 0.15 mmol) were dissolved in CH_2Cl_2 (50 mL). The solution was further stirred during 2 days at room temperature before evaporation, and the residue was washed with diethyl ether (3 × 25 mL). After crystallization in a dichloromethane/pentane mixture, 206 mg of dark purple crystals of [**3**][**OTf**] were obtained (65%). Complex *trans*-$[Cl(dppe)_2Ru{-}C{\equiv}C{-}C(Ph){=}CHPh]$ (**8d**) was identified as a coproduct with two diastereoisomers Z and E. $^{31}P\{^1H\}$ NMR ($CDCl_3$, 121.47 MHz, 297 K): δ = 49.9 and 44.6 (s, PPh_2). ^1H NMR ($CDCl_3$, 300.13 MHz, 297 K): δ = 7.65−6.75 (m, 45H, Ph), 6.35 (s, 1H, CH, 60%), 5.77 (s, 1H, CH, 40%), 2.85−2.45 (m, 8 H, CH_2). $^{13}C\{^1H\}$ NMR (75 MHz, CD_2Cl_2, 297 K): δ = 131.01 (quint., Ru−*C*≡C−, $^2J(P,C)$ = 14 Hz, the oher one is masked by the phenyl groups), 136.93−127.16 (Ph), 128.38 and 128.07 (Ru−C≡C−*C*), 128.26 and 126.63 (CH), 118.27 and 113.67 (Ru−C≡*C*−), 30.50 and 28.60 (m, PCH_2CH_2P, $|^1J(P,C) + {}^3J(P,C)|$ = 23 Hz). IR (KBr): υ = 2037 (C≡C), 1596 (C=C) cm^{-1}. HR-MS FAB$^+$ (*m*/*z*): 1136.2310 ([M]$^+$, calcd: 1136.2299).

***trans*-[Cl(dppe)$_2$Ru=C=C=C(CH$_3$)$_2$]BF$_4$ ([4a][BF$_4$]):** In a Schlenk tube, $[(dppe)_2RuCl]BF_4$ (400 mg, 0.4 mmol) and $(CH_3)_2C(OH){-}C{\equiv}CH$ (81 mg, 1.00 mmol) were dissolved in CH_2Cl_2 (40 mL). The solution was stirred during 18 h at room temperature. After filtration, the solution was evaporated and then the residue was washed with diethyl ether (3 × 25 mL). Further crystallization in a dichloromethane/pentane mixture led to 356 mg of dark crystals (82%). $^{31}P\{^1H\}$ NMR (121 MHz, CD_2Cl_2, 297 K): δ = 42.2 (s, PPh_2). ^1H NMR (300 MHz, CD_2Cl_2, 297 K): δ = 7.38−6.78 (m, 40H, Ph), 2.60−3.00 (m, 8 H, CH_2), 1.26 (s, 6H, CH_3). $^{13}C\{^1H\}$ NMR (75 MHz, CD_2Cl_2, 297 K): δ = 319.67 (quint., $^2J(P,C)$ = 14 Hz, C_α), 201.21 (s, C_β), 175.80 (s, C_γ), 133.75−127.87 (Ph), 35.86 (CH_3), 29.19 (m, PCH_2CH_2P, $|^1J(P,C) + {}^3J(P,C)|$ = 23 Hz, CH_2). IR (KBr): υ = 1958 (=C=C=C), 1059 (BF) cm^{-1}. HR-MS FAB$^+$ (*m*/*z*): 999.1928 ([M]$^+$, calcd: 999.1908). Elemental analysis (%) for $C_{57}H_{54}P_4F_4ClBRu$: C, 62.99; H, 5.22 (Calcd: C, 63.02; H, 5.01).

***trans*-[Cl(dppe)$_2$Ru=C=C=C(CH$_3$)$_2$]OTf ([4a][OTf]):** The procedure was identical with that for [**4a**][**BF$_4$**] with $[(dppe)_2RuCl]OTf$ (540 mg, 0.54 mmol) and $(CH_3)_2C(OH){-}C{\equiv}CH$ (81 mg, 1.00 mmol) and yielded 526 mg of dark crystals (85%).$^{31}P\{^1H\}$ NMR (121 MHz, CD_2Cl_2, 297 K): δ = 42.3 (s, PPh_2). ^1H NMR (300 MHz, CD_2Cl_2, 297 K): δ = 7.41−6.95 (m, 40H, Ph), 2.60−3.00 (m, 8 H, CH_2), 1.26 (s, 6H, CH_3). $^{13}C\{^1H\}$ NMR (75 MHz, CD_2Cl_2, 297 K): δ = 318.81 (quint., $^2J(P,C)$ = 14 Hz, C_α), 200.90 (quint., $^2J(P,C)$ = 2.5 Hz, C_β), 173.88 (s, C_γ), 132.66−126.83 (Ph), 34.82 (CH_3), 28.17 (m, PCH_2-

(72) National Institute of Environmental Health Sciences, Public EPR Software Tools, version 0.98. http://EPR.niehs.nih.gov/.
(73) Chaudret, B.; Commengues, G.; Poilblanc, R. *J. Chem. Soc., Dalton Trans.* **1984**, 1635−1639.
(74) Polam, J. R.; Porter, L. C. *J. Coord. Chem.* **1993**, *29*, 109−119.
(75) O'Hagan, D.; Zaidi, N. A. *J. Chem. Soc., Perkin Trans. 1* **1992**, 947−949.
(76) ADF2004.01, Theoretical Chemistry, Vrije Universiteit: Amsterdam, The Netherlands, SCM.
(77) (a) Baerends, E. J.; Ellis, D. E.; Ros, P. *Chem. Phys.* **1973**, *2*, 41−51. (b) te Velde, G.; Baerends, E. J. *J. Comput. Phys.* **1992**, *99*, 84−98. (c) Fonseca Guerra, C.; Snijders, J. G.; te Velde, G.; Baerends, E. J. *Theor. Chem. Acc.* **1998**, *99*, 391−403. (d) Bickelhaupt, F. M.; Baerends, E. J. *Rev. Comput. Chem.* **2000**, *15*, 1−86. (e) te Velde, G.; Bickelhaupt, F.; Fonseca Guerra, C.; van Gisbergen, S. J. A.; Baerends, E. J.; Snijders, J. G.; Ziegler, T. *J. Comput. Chem.* **2001**, *22*, 931−967.
(78) (a) Vosko, S. D.; Wilk, L.; Nusair, M. *Can. J. Chem.* **1990**, *58*, 1200−1211. (b) Becke, A. D. *J. Chem. Phys.* **1986**, *84*, 4524−4529. (c) Becke, A. D. *Phys. Rev. A* **1988**, *38*, 3098−3100. (d) Perdew, J. P. *Phys. Rev. B* **1986**, *33*, 8822−8824. *Ibid 34*, 7406.
(79) Verluis, L.; Ziegler, T. *J. Chem. Phys.* **1988**, *88*, 322−328.
(80) Flükiger, P.; Lüthi, H. P.; Portmann, S.; Weber, J. *Molekel 4.1*; Swiss Center for Scientific Computing: Manno, 2002.

CH_2P, $|^1J(P,C) + {}^3J(P,C)| = 23$ Hz, CH_2). IR (KBr): $\upsilon = 1959$ (=C=C=C) cm^{-1}. HR-MS FAB$^+$ (*m*/*z*): 999.1935 ([M]$^+$, calcd: 999.1908).

***trans*-[Cl(dppe)$_2$Ru=C=C=C(CH$_3$)Ph]BF$_4$ ([4b][BF$_4$]):** The procedure was identical with that for [**4a**][**BF$_4$**] with [(dppe)$_2$RuCl]BF$_4$ (408 mg, 0.4 mmol) and Ph(CH$_3$)C(OH)-C≡CH (147 mg, 1.00 mmol) and yielded 417 mg of dark red crystals (91%). $^{31}P\{^1H\}$ NMR (121 MHz, CD_2Cl_2, 297 K): $\delta = 40.4$ (s, PPh_2). ^1H NMR (300 MHz, CD_2Cl_2, 297 K): $\delta = 7.60-7.00$ (m, 45H, Ph), 2.70−3.2 (m, 8 H, CH_2), 1.55 (s, 3H, CH_3). $^{13}C\{^1H\}$ NMR (75 MHz, CD_2Cl_2, 297 K): $\delta =$ 310.57 (quint., $^2J(P,C) = 14$ Hz, C_α), 210.19 (s, C_β), 162.18 (s, C_γ), 142.88−128.26 (Ph), 31.94 (CH_3), 29.06 (m, PCH_2CH_2P, $|^1J(P,C) + {}^3(P,C)| = 23$ Hz, CH_2). IR (KBr): $\upsilon = 1932$ (=C=C=C), 1056 (BF) cm^{-1}. HR-MS FAB$^+$ (*m*/*z*): 1061.2076 ([M]$^+$, calcd: 1061.2079). Elemental analysis (%) for $C_{62}H_{56}P_4F_4ClBRu$: C, 64.82; H, 5.05 (Calcd: C, 64.85; H, 4.92).

***trans*-[Cl(dppe)$_2$Ru=C=C=C(CH$_2$CH$_3$)Ph]BF$_4$ ([4c][BF$_4$]):** The procedure was identical with that for [**4a**][**BF$_4$**] with [(dppe)$_2$RuCl]-BF_4 (306 mg, 0.30 mmol) and Ph(C_2H_5)C(OH)−C≡CH (112 mg, 0.75 mmol) and yielded 280 mg of dark red crystals (80%). $^{31}P\{^1H\}$ NMR (121 MHz, CD_2Cl_2, 297 K): $\delta = 40.1$ (s, PPh_2). ^1H NMR (300 MHz, CD_2Cl_2, 297 K): $\delta = 7.55-6.82$ (m, 45H, Ph), 2.70−3.20 (m, 8 H, CH_2), 2.24 (quad., $^3J(H,H) = 7$ Hz, 2H, CH_2), 1.10 (t., $^3J(H,H) = 7$ Hz, 3H, CH_3). $^{13}C\{^1H\}$ NMR (75 MHz, CD_2Cl_2, 297 K): $\delta = 311.76$ (quint., $^2J(P,C) = 14$ Hz, C_α), 210.02 (s, C_β), 169.75 (s, C_γ), 142.81−128.24 (Ph), 38.51 (CH_2−CH_3), 29.27 (m, PCH_2CH_2P, $|^1J(P,C) + {}^3J(P,C)| = 23$ Hz, CH_2), 12.75 (CH_3). IR (KBr): $\upsilon = 1933$ (=C=C=C), 1979, $\upsilon = 1062$ (BF) cm^{-1}. HR-MS FAB$^+$ (*m*/*z*): 1075.2231 ([M]$^+$, calcd: 1075.2236). Elemental analysis (%) for $C_{63}H_{58}P_4F_4ClBRu$: C, 65.14; H, 5.11 (Calcd: C, 65.10; H, 5.03).

***trans*-[Cl(dppe)$_2$Ru=C=C=C(CH$_2$Ph)Ph]OTf ([4d][OTf]):** The procedure was identical with that for [**4a**][**BF$_4$**] with [(dppe)$_2$RuCl]-OTf (540 mg, 0.54 mmol) and $PhCH_2$(Ph)C(OH)−C≡CH (290 mg, 1.2 mmol) and yielded 528 mg of dark crystals (80%). $^{31}P\{^1H\}$ NMR (121 MHz, CD_2Cl_2, 297 K): $\delta = 42.4$ (s, PPh_2). ^1H NMR (300 MHz, CD_2Cl_2, 297 K): $\delta = 7.75-6.75$ (m, 50H, Ph), 3.45 (s, 2H, CH_2), 2.60−3.10 (m, 8 H, CH_2). $^{13}C\{^1H\}$ NMR (75 MHz, CD_2Cl_2, 297 K): $\delta = 311.4$ (quint., $^2J(P,C) = 14$ Hz, C_α), 215.4 (s, C_β), 162.66 (s, C_γ), 142.90−127.10 (Ph), 48.87 (CH_2), 29.12 (m, PCH_2CH_2P, $|^1J(P,C) + {}^3J(P,C)| = 23$ Hz, CH_2). IR (KBr): $\upsilon = 1929$ (=C=C=C). HR-MS FAB$^+$ (*m*/*z*): 1137.2390 ([M]$^+$, calcd: 1137.2378). Elemental analysis (%) for $C_{68}H_{60}P_4F_3ClO_3SRu$: C, 64.25; H, 5.01 (Calcd: C, 64.07; H, 4.75).

***trans*-[Cl(dppe)$_2$Ru=C=C=C(CH$_3$)−CH=C(CH$_3$)−C≡C−Ru-(dppe)$_2$Cl]BF$_4$ ([5a][BF$_4$]):** In a Schlenk tube, [**4a**][**BF$_4$**] (200 mg, 0.17 mmol) was dissolved in CH_2Cl_2 (30 mL). In another tube, **2b** (184 mg, 0.17 mmol) was dissolved in CH_2Cl_2 (100 mL). This solution was slowly added to the first one over 3 days using a dropping funnel. This mixture was further stirred during 3 days at room temperature. After filtration, the solution was evaporated, and then the residue was washed with diethyl ether (3 × 25 mL). Crystallizations in a CH_2Cl_2/pentane mixture yielded 306 mg of dark green crystals (85%). $^{31}P\{^1H\}$ NMR (121 MHz, CD_2Cl_2, 297 K): $\delta = 47.1$ (s, PPh_2). ^1H NMR (300 MHz, CD_2Cl_2, 297 K): $\delta = 7.35-6.95$ (m, 80H, Ph), 5.50 (s, 1H, CH), 2.40−2.90 (m, 16 H, CH_2), 1.35 (s, 6H, CH_3). $^{13}C\{^1H\}$ NMR (75 MHz, CD_2Cl_2, 297 K): $\delta = 224.20$ (quint., $^2J(P,C) = 14$ Hz, C_α), 157.10 (s, C_β), 152.50 (s, CH), 137.4 (s, C_γ), 135.65−127.76 (Ph), 30.20 (m, PCH_2CH_2P, $|^1J(P,C) + {}^3J(P,C)| = 23$ Hz, CH_2), 29.74 (CH_3). IR (KBr): $\upsilon = 1903$ (=C=C=C), 1995, 1054 (BF) cm^{-1}. HR-MS FAB$^+$ (*m*/*z*): 1981.3527 ([M]$^+$, calcd: 1981.3463). Elemental analysis (%) for $C_{113}H_{103}P_8Cl_2Ru_2BF_4$: C, 65.85; H, 5.18 (Calcd: C, 65.61; H, 5.02).

***trans*-[Cl(dppe)$_2$Ru=C=C=C(CH$_3$)−CH=C(Ph)−C≡C−Ru(dppe)$_2$Cl]BF$_4$ ([5b][BF$_4$]):** The procedure was identical with that for [**5a**][**BF$_4$**] with [**4b**][**BF$_4$**] (200 mg, 0.17 mmol) and acetylide **2b** (174 mg, 0.05 mmol) and yielded 352 mg of dark green crystals (79%). $^{31}P\{^1H\}$ NMR (121 MHz, CD_2Cl_2, 297 K): $\delta = 47.0$ (s, PPh_2), 49.7 (s, PPh_2). ^1H NMR (300 MHz, CD_2Cl_2, 297 K): $\delta = 7.41-6.83$ (m, 85H, Ph), 5.79 (s, 1H, CH), 2.40−2.90 (m, 16 H, CH_2), 0.92 (s, 3H, CH_3). $^{13}C\{^1H\}$ NMR (75 MHz, CD_2Cl_2, 297 K): $\delta = 230.21$ and 223.95 (quint., $^2J(P,C) = 14$ Hz, C_α and $C_{\alpha'}$), 162.61 (s, $C_{\beta'}$ methyl side), 162.22 (s, C_β phenyl side), 153.61 ($C_{\gamma'}$ methyl side), 145.76 (s, C_γ phenyl side), (s, C_γ and $C_{\gamma'}$), 137.91 (s, CH), 151.73−127.71 (Ph), 30.83 and 29.78 (m, PCH_2CH_2P, $|^1J(P,C) + {}^3J(P,C)| = 23$ Hz, CH_2), 25.97 (CH_3). IR (KBr): $\upsilon = 1897$ (=C=C=C), 1988, 1054 (BF) cm^{-1}; HR-MS FAB$^+$ (*m*/*z*): 2043.3657 ([M]$^+$, calcd: 2043.3581). Elemental analysis (%) for $C_{118}H_{105}P_8Cl_2Ru_2BF_4$: C, 66.26; H, 5.31 (Calcd: C, 66.52; H, 4.97).

***trans*-[Cl(dppe)$_2$Ru=C=C=C(CH$_3$)−C(CH$_3$)=C(Ph)−C≡C−Ru(dppe)$_2$Cl]BF$_4$ ([5c][BF$_4$]):** The procedure was identical with that for [**5a**][**BF$_4$**] with **4b** (200 mg, 0.16 mmol) and acetylide **2b** (172 mg, 0.2 mmol) and yielded 287 mg of dark green crystals (82%). $^{31}P\{^1H\}$ NMR (121 MHz, CD_2Cl_2, 297 K): $\delta = 49.6$ (s, PPh_2), 43.8 (s, PPh_2). ^1H NMR (300 MHz, CD_2Cl_2, 297 K): $\delta = 7.68-6.40$ (m, 85H, Ph), 2.40−3.00 (m, 16 H, CH_2), 1.27 (s, 3H, central CH_3), 1.06 (s, 3H, other CH_3). $^{13}C\{^1H\}$ NMR (75 MHz, CD_2Cl_2, 297 K): $\delta = 245.26$ and 220.37 (quint., $^2J(P,C) = 14$ Hz, C_α and $C_{\alpha'}$), 170.47 (s, C_β phenyl side), 158.22 (s, $C_{\beta'}$ methyl side), 157.99 (s, C_γ phenyl side), 146.64 ($C_{\gamma'}$ methyl side), 152.11 (s, C_δ−CH_3), 145.52−127.56 (Ph), 31.01 and 28.97 (m, PCH_2CH_2P, $|^1J(P,C) + {}^3J(P,C)| = 23$ Hz, CH_2), 30.70 (s, C_γ−CH_3), 22.47 (C_δ−CH_3), IR (KBr): $\upsilon = 1889$ (=C=C=C), 1981, 1055 (BF) cm^{-1}. HR-MS FAB$^+$ (*m*/*z*): 2058.3908 ([M]$^+$, calcd: 2058.3781). Elemental analysis (%) for $C_{119}H_{107}P_8Cl_2Ru_2BF_4$: C, 66.49; H, 5.06 (Calcd: C, 66.64; H, 5.03).

***trans*-[Cl(dppe)$_2$Ru=C=C=C(CH$_3$)−CH=C(CH$_3$)−C≡C−C≡C−Ru(dppe)$_2$Cl]BF$_4$ ([7][OTf]):** In a Schlenk tube, [**4a**][**OTf**] (173 mg, 0.16 mmol) was dissolved in CH_2Cl_2 (30 mL). In another tube, acetylide **6** (184 mg, 0.16 mmol) was also dissolved in CH_2Cl_2 (100 m)L. This solution was slowly added to the first one over 3 days using a dropping funnel. This mixture was further stirred during 19 days at room temperature. After filtration, the solution was evaporated, and then the residue was washed with diethyl ether (3 × 25 mL). Crystallizations in a CH_2Cl_2/pentane mixture yielded 169 mg of dark purple crystals of **7** (49%). $^{31}P\{^1H\}$ NMR (121 MHz, CD_2Cl_2, 297 K): $\delta = 48.4$ and 43.9 (s, PPh_2). ^1H NMR (300 MHz, CD_2Cl_2, 297 K): $\delta = 7.50-6.82$ (m, 80H, Ph), 4.91 (s, 1H, CH), 2.40−2.40 (m, 16 H, CH_2), 2.03 (s, 3H, CH_3), 1.64 (s, 3H, CH_3). $^{13}C\{^1H\}$ NMR (75 MHz, CD_2Cl_2, 297 K): $\delta = 243.53$ (Ru=*C*), 186.13 (Ru=C=*C*), 152.44 (CH), 141.83 (Ru=C=C=*C*), 135.71−127.56 (Ph), 121.41 (quad., CF3, $^1J(C,F) = 321$ Hz), 119.28 (Ru−C≡C−*C*≡C, Ru−*C*≡C and Ru−C≡*C* not observed), 108.95 (Ru−C≡C−C≡*C*), 91.30 (C≡C−*C*(CH_3), 31.02 and 30.44 (m, PCH_2CH_2P, $|^1J(P,C) + {}^3J(P,C)| = 23$ Hz), 29.08 (Ru≡C−CH=C(*C*H$_3$)), 21.72 (C_δ−*C*H$_3$). IR (KBr): $\upsilon = 1893$ (=C=C=C), 2078 (C≡C), 2023, 1963 cm^{-1}; HR-MS FAB$^+$ (*m*/*z*): 2005.3439 ([M]$^+$, calcd: 2005.3425).

***trans*-[Cl(dppe)$_2$Ru−C≡C−C(=CH$_2$)−CH(CH$_3$)=C(CH$_3$)−C≡C−Ru(dppe)$_2$Cl] (9a).** In a Schlenk tube, [**5a**][**BF$_4$**] (40 mg, 0.02 mmol) was dissolved in CH_2Cl_2 (10 mL). Slow addition of a DBU solution (4.9 mL, 4×10^{-6} mol L^{-1}) led to the discoloration of the green solution. After further stirring for 1 h at room temperature, the mixture was evaporated to dryness. The brown solid was washed with pentane (10 mL). $^{31}P\{^1H\}$ NMR (121 MHz, CD_2Cl_2, 297 K): $\delta =$ 51.0 and 49.8 (s, PPh_2). ^1H NMR (300 MHz, CD_2Cl_2, 297 K): $\delta =$ 8.01−6.78 (m, 80H, Ph), 5.48 (s, 1H), 4.70 (d, 1H, CH, $^2J(H,H) = 3.3$ Hz), 4.65 (d, 1H, CH, $^2J(H,H) = 3.3$ Hz), 2.40−2.90 (m, 16 H, CH_2), 1.73 (s, 3H, CH_3). $^{13}C\{^1H\}$ NMR (75 MHz, CD_2Cl_2, 297 K): $\delta =$ 137.55−126.49 (Ph), 124.19 (Ru−C≡C−*C*CH$_3$), 127.83 (CH), 119.56 (quint., Ru−*C*≡C, $^2J(P,C) = 15$ Hz, only one C_α is observed), 118.50 (Ru−C≡*C*−CCH$_3$, only one C_β is observed), 114.45 (=CH_2), 115.10 (Ru−C≡C−*C*=CH_2), 30.77 and 30.60 (m, PCH_2CH_2P, $|^1J(P,C) + {}^3J(P,C)| = 23$ Hz), 26.54 (CH_3). IR (KBr): $\upsilon = 2045$ (C≡C), 1645 (C=C) cm^{-1}.

***trans*-[Cl(dppe)$_2$Ru−C≡C−C(=CH$_2$)−C(CH$_3$)=CPh−C≡C−**

Ru(dppe)$_2$Cl] (9c). In a Schlenk tube, [**5c**][**BF$_4$**] (40 mg, 0.02 mmol) was dissolved in CH_2Cl_2 (10 mL). Slow addition of a DBU solution (4.8 mL, 4×10^{-6} mol L^{-1}) led to the discoloration of the green solution. After further stirring for 1 h at room temperature, the mixture was evaporated to dryness. The brown solid was washed with pentane (10 mL). $^{31}P\{^1H\}$ NMR (121 MHz, CD_2Cl_2, 297 K): $\delta = 52.3$ and 52.1 (s, PPh_2). ^1H NMR (300 MHz, CD_2Cl_2, 297 K): $\delta = 7.96-6.69$ (m, 85H, Ph), 4.73 (d, 1H, CH, ^2J(H,H) = 2.9 Hz), 4.31 (d, 1H, CH, ^2J(H,H) = 2.9 Hz), 2.40−2.90 (m, 16 H, CH_2), 1.56 (s, 3H, CH_3). $^{13}C\{^1H\}$ NMR (75 MHz, CD_2Cl_2, 297 K): $\delta = 143.79-124.21$ (Ph), 136.9 (Ru−C≡C−*C*═CH_2), 129.62 (Ru−C≡C−*C*Ph), 124.15 (*C*−CH_3), 119.19 (quint., Ru−*C*≡C, ^2J(P,C) = 15 Hz, only one C_α is observed), 117.65 (Ru−C≡*C*−CPh), 116.18 (═CH_2), 115.97 (Ru−C≡*C*−C═CH_2), 31.24 and 30.79 (m, PCH_2CH_2P, $|^1J(P,C) + {}^3J(P,C)| = 21$ Hz), 21.27 (CH_3). IR (KBr): $\upsilon = 2045$, 2022 (C≡C), 1647 (C═C) cm^{-1}.

***trans*-[Cl(dppe)$_2$Ru═C═CH−C(CH$_3$)═CH−C(CH$_3$)═C═C═Ru(dppe)$_2$Cl](BF$_4$)$_2$ ([10a][BF$_4$]$_2$).** In a Schlenk tube, [**5a**][**BF$_4$**] (40 mg, 0.02 mmol) was dissolved in CH_2Cl_2 (5 mL). Slow addition of a HBF_4·Et_2O solution (3.0 mL, 7.2×10^{-3} mol L^{-1}) in CH_2Cl_2 led to a deep blue coloration. After further stirring for 15 min at room temperature, the mixture was evaporated to dryness. The blue solid was washed with diethyl ether (2 × 10 mL), and 34 mg of [**10a**][**BF$_4$**]$_2$ were recovered (85%). $^{31}P\{^1H\}$ NMR (121 MHz, CD_2Cl_2, 297 K): $\delta = 41.1$ and 32.9 (s, PPh_2). ^1H NMR (300 MHz, CD_2Cl_2, 297 K): $\delta = 7.55-6.85$ (m, 80H, Ph), 6.04 (s, 1H, C_δH), 5.96 (s, 1H, Ru═C═CH), 3.30−3.00 (m, 16 H, CH_2), 0.03 (s, 3H, CH_3), −0.78 (s, 3H, CH_3). $^{13}C\{^1H\}$ NMR (75 MHz, CD_2Cl_2, 297 K): $\delta = 336.31$ (quint., Ru═*C*═CH, ^2J(P,C) = 15 Hz, Ru═*C*═C═C not observed), 191.75 (Ru═C═*C*═C(CH_3)), 159.53 (Ru═C═C═*C*(CH_3)), 154.33 (Ru═C═CH−*C*), 128.84 (C_δH), 134.28−127.78 (Ph), 120.20 (Ru═C═*C*H), 29.50 and 29.97 (m, PCH_2CH_2P, $|^1J(P,C) + {}^3J(P,C)| = 21$ Hz), 31.62 (Ru═C═C═C(*C*H_3)), 21.46 (Ru═C═CH−C(*C*H_3)). IR (KBr): $\upsilon = 1912$ (C═C═C) cm^{-1}.

***trans*-[Cl(dppe)$_2$Ru═C═CH−C(CH$_3$)═C(CH$_3$)CPh═C═C═Ru(dppe)$_2$Cl](BF$_4$)$_2$ ([10c][BF$_4$]$_2$).** In a Schlenk tube, [**5c**][**BF$_4$**] (40 mg, 0.02 mmol) was dissolved in CH_2Cl_2 (5 mL). Slow addition of a HBF_4·Et_2O solution (3.0 mL, 7.2×10^{-3} mol L^{-1}) in CH_2Cl_2 led to a deep blue coloration. After further stirring for 15 min at room temperature, the mixture was evaporated to dryness. The blue solid was washed with diethylether (2 × 10 mL), and 32 mg of [**10c**][**BF$_4$**]$_2$ were recovered (85%). $^{31}P\{^1H\}$ NMR (121 MHz, CD_2Cl_2, 297 K): $\delta = 42.9$ and 37.6 (s, PPh_2). ^1H NMR (300 MHz, CD_2Cl_2, 297 K): $\delta = 7.55-6.23$ (m, 85H, Ph), 4.25 (s, 1H, CH), 3.15−2.70 (m, 16 H, CH_2), 1.29 (s, 3H, C_δ−*C*H_3), −0.37 (s, 3H, C_γ−CH_3). $^{13}C\{^1H\}$ NMR (75 MHz, CD_2Cl_2, 297 K): $\delta = 345.47$ (quint., Ru═*C*═CH, ^2J(P,C) = 15 Hz), 284.16 (quint., Ru═*C*═C═CPh, ^2J(P,C) = 15 Hz), 204.47 (Ru═C═*C*═CPh), 161.40 (Ru═C═C═*C*Ph), 145.06 (Ru═C═CH−*C*), 136.85 (C_δ), 148.06−127.00 (Ph), 115.82 (Ru═C═*C*H), 29.14 and 28.99 (m, PCH_2CH_2P, $|^1J(P,C) + {}^3J(P,C)| = 21$ Hz), 25.22 (C_γ−*C*H_3), 20.71 (C_δ−*C*H_3). IR (KBr): $\upsilon = 1905$ (C═C═C) cm^{-1}.

***trans*-[Cl(dppe)$_2$Ru≡C−CH═C(CH$_3$)−CH═C(CH$_3$)−HC═C═Ru(dppe)$_2$Cl](BF$_4$)$_3$ ([11a][BF$_4$]$_3$).** In an NMR tube containing [**5a**][**BF$_4$**] (8 mg, 0.01 mmol) and CD_2Cl_2 (0.5 mL), HBF_4·Et_2O (54% in Et_2O, 5 μL, 4 equiv) was added. The blue solution turned to purple. $^{31}P\{^1H\}$ NMR (121 MHz, CD_2Cl_2, 297 K): $\delta = 34.6$ (s, PPh_2). ^1H NMR (300 MHz, CD_2Cl_2, 297 K): $\delta = 7.70-5.80$ (m, 85H, Ph), 6.25 (s, 1H, C_δH), 5.95 (s, 2H, C_βH), 3.10−2.70 (m, 16 H, CH_2), −0.74 (s, 6H, CH_3). $^{13}C\{^1H\}$ NMR (75 MHz, CD_2Cl_2, 297 K): $\delta =$ (C_α not observed), 170.72 (C_γ), 134.05−128.55 (Ph), 124.21 (C_β), 120.19 (C_δ), 28.98 (m, PCH_2CH_2P, $|^1J(P,C) + {}^3J(P,C)| = 21$ Hz), 21.37 (CH_3).

***trans*-[Cl(dppe)$_2$Ru≡C−CH═C(CH$_3$)−C(CH$_3$)═CPh−HC═C═Ru(dppe)$_2$Cl](BF$_4$)$_3$ ([11c][BF$_4$]$_3$).** In an NMR tube containing [**5c**][**BF$_4$**] (10 mg, 0.01 mmol) and CD_2Cl_2 (0.5 mL), HBF_4·Et_2O (54% in Et_2O, 10 μL, 8 equiv) was added. The blue solution turned to purple. $^{31}P\{^1H\}$ NMR (121 MHz, CD_2Cl_2, 297 K): $\delta = 39.3$ and 34.6 (s, PPh_2). ^1H NMR (300 MHz, CD_2Cl_2, 297 K): $\delta = 7.70-5.80$ (m, 85H, Ph), 5.16 (s, 1H, Ru≡C−CH), 4.60 (s, 1H, Ru═C═CH), 3.15−2.70 (m, 16 H, CH_2), 1.48 (s, 3H, CH_3), −0.94 (s, 3H, CH_3). $^{13}C\{^1H\}$ NMR (75 MHz, CD_2Cl_2, 297 K): $\delta = 326.10$ (Ru≡*C*−CH, Ru═C═CH not observed), 172.67 (Ru≡C−CH═*C*(CH_3)), 163.68 (Ru═C═CH−*C*Ph), 130.86 (C_δ), 124.56 (Ru≡C−*C*H), 140.47−127.61 (Ph), 119.60 (Ru═C═*C*H), 28.63 and 27.92 (m, PCH_2CH_2P, $|^1J(P,C) + {}^3J(P,C)| = 22$ Hz), 25.49 (Ru≡C−CH═C(*C*H_3)), 22.98 (C_δ−*C*H_3).

Acknowledgment. We thank the CNRS and the Université de Rennes 1 for support, Dr. Claude Lapinte (UMR 6226) for helpful discussions, and Dr. Pierre Guénot from the Centre Régional de Mesures Physiques de l'Ouest (Rennes) for structure determination. DFT calculations were carried out at the PCIO (Rennes), the IDRIS-CNRS (Orsay), and at the CINES-MENESR (Montpellier).

Supporting Information Available: Calculated Atomic Mulliken charges, and EPR spectra of **3a**, **5c**, [**3**]$^{2+}$, and [**5a**,**c**]$^{2+}$. This material is available free of charge via the Internet at http://pubs.acs.org.

JA0603453